

## Reporting Summary

Nature Portfolio wishes to improve the reproducibility of the work that we publish. This form provides structure for consistency and transparency in reporting. For further information on Nature Portfolio policies, see our [Editorial Policies](#) and the [Editorial Policy Checklist](#).

### Statistics

For all statistical analyses, confirm that the following items are present in the figure legend, table legend, main text, or Methods section.

n/a Confirmed

- The exact sample size ( $n$ ) for each experimental group/condition, given as a discrete number and unit of measurement
- A statement on whether measurements were taken from distinct samples or whether the same sample was measured repeatedly
- The statistical test(s) used AND whether they are one- or two-sided  
*Only common tests should be described solely by name; describe more complex techniques in the Methods section.*
- A description of all covariates tested
- A description of any assumptions or corrections, such as tests of normality and adjustment for multiple comparisons
- A full description of the statistical parameters including central tendency (e.g. means) or other basic estimates (e.g. regression coefficient) AND variation (e.g. standard deviation) or associated estimates of uncertainty (e.g. confidence intervals)
- For null hypothesis testing, the test statistic (e.g.  $F$ ,  $t$ ,  $r$ ) with confidence intervals, effect sizes, degrees of freedom and  $P$  value noted  
*Give  $P$  values as exact values whenever suitable.*
- For Bayesian analysis, information on the choice of priors and Markov chain Monte Carlo settings
- For hierarchical and complex designs, identification of the appropriate level for tests and full reporting of outcomes
- Estimates of effect sizes (e.g. Cohen's  $d$ , Pearson's  $r$ ), indicating how they were calculated

*Our web collection on [statistics for biologists](#) contains articles on many of the points above.*

### Software and code

Policy information about [availability of computer code](#)

Data collection CryoEM data were collected using the EPU software version 3.2.0.4775REL (FEI, Netherlands) using AutoCTF function of Sherpa (version 2.11.1)

Data analysis RELION v 4 with MotionCor2 v1.2.1 and CTFIND 4.1.14 were used for processing micrographs, picking particles, classification and refining cryo-EM maps. RELION was used to calculate local resolution. Coot v0.9.8.92 for model building and ServalCat v0.3.1 with REFMAC 5 v5.8.0415 for model refinement and statistics, with structural restraints generated by aceDRG. Figures were generated using ChimeraX v1.9. Validation was performed using Phenix 1.20-4487.

MD simulations were prepared, performed and analyzed using GROMACS 2025 with the implemented LINCS and GENION versions. For preparation WHATIF 20071220-093 was used. Overlap volume calculation for MD trajectories was scripted in Python 3.13. Functional mode analysis was conducted with a GROMACS branch that can be downloaded at [https://www3.mpiibpc.mpg.de/groups/de\\_groot/fma.html](https://www3.mpiibpc.mpg.de/groups/de_groot/fma.html). Figures with MD simulation results were created with R 4.5.1 and ChimeraX 1.10.1.

For manuscripts utilizing custom algorithms or software that are central to the research but not yet described in published literature, software must be made available to editors and reviewers. We strongly encourage code deposition in a community repository (e.g. GitHub). See the Nature Portfolio [guidelines for submitting code & software](#) for further information.

## Data

Policy information about [availability of data](#)

All manuscripts must include a [data availability statement](#). This statement should provide the following information, where applicable:

- Accession codes, unique identifiers, or web links for publicly available datasets
- A description of any restrictions on data availability
- For clinical datasets or third party data, please ensure that the statement adheres to our [policy](#)

The raw sequencing reads from the deep mutational scanning have been deposited in the DDBJ under BioProject accession number PRJDB39765. The cryo-electron microscopy maps and the respective coordinates for electron-microscopy-based model have been deposited in the EMDDataBank and PDB under the accession numbers EMD50855, EMD50856 and E MD50858 and PDB ID 9FY1, 9FY2 and 9FY3.

MD simulation input files, final coordinates and analyses are available on zenodo.org (<https://doi.org/10.5281/zenodo.17779011>).

The following structures from the PDB were used for reasons of figure preparation and comparison: 9MTP, 8QOA, 5NWY, 7O19, 5A81, 8CVK and 7NSO.

## Research involving human participants, their data, or biological material

Policy information about studies with [human participants or human data](#). See also policy information about [sex, gender \(identity/presentation\), and sexual orientation](#) and [race, ethnicity and racism](#).

Reporting on sex and gender	<input type="text" value="N/A"/>
Reporting on race, ethnicity, or other socially relevant groupings	<input type="text" value="N/A"/>
Population characteristics	<input type="text" value="N/A"/>
Recruitment	<input type="text" value="N/A"/>
Ethics oversight	<input type="text" value="N/A"/>

Note that full information on the approval of the study protocol must also be provided in the manuscript.

## Field-specific reporting

Please select the one below that is the best fit for your research. If you are not sure, read the appropriate sections before making your selection.

- Life sciences       Behavioural & social sciences       Ecological, evolutionary & environmental sciences

For a reference copy of the document with all sections, see [nature.com/documents/nr-reporting-summary-flat.pdf](https://www.nature.com/documents/nr-reporting-summary-flat.pdf)

## Life sciences study design

All studies must disclose on these points even when the disclosure is negative.

Sample size	No sample size calculation was performed. The sample size was selected on the basis of a two-day data collection, which was chosen to obtain sufficient number of particles to bring the resolution of the resulting complexes towards 2Å resolution.
Data exclusions	Micrographs with low estimated resolution or poorly fitted CTFs were discarded, as were particles that clustered into poorly defined classes during 2D and 3D classification.
Replication	For b-galactosidase assay, three or six biological replicates were averaged. For in vitro translation arrest assay and toeprinting, one of at least two biological replicates are presented.
Randomization	For 3D refinement in RELION, particles are randomly placed in one of two subsets. These subsets are maintained for CTF refinement. Otherwise, no randomization was performed. For the molecular dynamics simulations, to obtain statistical uncertainties, 1000 subsets of conformations were randomly selected and the analysis was repeated on each subset.
Blinding	No blinding was performed as blinding is not possible or not applicable for the experiments because the identity of the analyzed sample was known.

## Reporting for specific materials, systems and methods

We require information from authors about some types of materials, experimental systems and methods used in many studies. Here, indicate whether each material, system or method listed is relevant to your study. If you are not sure if a list item applies to your research, read the appropriate section before selecting a response.

## Materials &amp; experimental systems

## Methods

- n/a Involved in the study
- Antibodies
- Eukaryotic cell lines
- Palaeontology and archaeology
- Animals and other organisms
- Clinical data
- Dual use research of concern
- Plants

- n/a Involved in the study
- ChIP-seq
- Flow cytometry
- MRI-based neuroimaging

## Antibodies

Antibodies used	anti-GFP antibody (Wako, 012-22541, clone mFX75)
Validation	The specificity of the anti-GFP antibody was validated by Western blotting in this study, showing that the size of the proteins detected by the antibodies were equivalent to the size of target proteins synthesized in vitro using specific DNA templates encoding the target proteins.

## Plants

Seed stocks	N/A
Novel plant genotypes	N/A
Authentication	N/A

# Diverse mechanisms of translation arrest by a Clostridia ribosome stalling peptide CliM

Corresponding Author: Professor Daniel Wilson

This file contains all reviewer reports in order by version, followed by all author rebuttals in order by version.

Version 0:

Reviewer comments:

Reviewer #1

(Remarks to the Author)

The manuscript reports a comprehensive analysis, using structural, biochemical, and mutational approaches, of the stalling mechanisms of the CliM stalling peptide. CliM is a membrane-insertion-sensing arrest peptide that couples YidC activity to feedback regulation of yidC expression. YidC is a membrane protein insertase in bacteria that helps newly synthesized membrane proteins insert into, and fold within, the lipid bilayer. As I described below, the study is strong with almost every conclusion supported by two or more experimental approaches. I just have a few small comments and suggestions regarding experiments in Fig 1, toeprinting experiments in Fig 2, and the cryo-EM section. I am describing these concerns below in the context of the specific experiments.

1. The authors demonstrate that CliM is a bona fide YidC-monitoring arrest peptide that regulates downstream yidC2 expression in response to membrane insertase activity. Using reporter assays in *B. subtilis*, they show that inhibition of CliM membrane insertion enhances yidC2 expression in an arrest-dependent manner, while successful insertion releases arrest. mRNA secondary structure analysis reveals that a stem-loop downstream of cliM mediates this regulation by coupling ribosome stalling to yidC2 translation. In Figure 1, the authors validate the proposed regulatory model in which CliM functions as a YidC activity sensor. Using *spolIIIJ*<sup>+</sup> (wild-type YidC1) and  $\Delta$ *spolIIIJ* backgrounds as readouts of membrane-insertion capacity, the authors show that loss of *SpolIIIJ* selectively induces yidC2 expression in an arrest-dependent manner (Fig. 1b), while efficient insertion in the *spolIIIJ*<sup>+</sup> background relieves CliM stalling (Fig. 1c). Arrest-deficient CliM mutants abolish yidC2 induction even when *SpolIIIJ* is absent, demonstrating that translational stalling, rather than *SpolIIIJ* deletion per se, drives the response. Dissection of the downstream mRNA stem-loop (Fig. 1d) further shows how ribosome stalling is transduced into increased yidC2 translation, completing the regulatory circuit. Together, these experiments convincingly establish that CliM couples YidC activity to feedback regulation of yidC2 expression. These are the main experiments in the paper to validate the YidC2 regulatory model.

While these results support the proposed model, I would have expected a bigger difference in beta-galactose activity for the wild type construct between *spolIIIJ*<sup>+</sup> and  $\Delta$ *spolIIIJ* in Fig 1b. Why does the wt construct in the *spolIIIJ*<sup>+</sup> produce so much signal if, in principle, there should be efficient CliM insertion, consequent arrest release, and thus low yidC2 expression? Also, how do the authors know that the key arrest-deficient mutations are solely affecting arrest and they are not altering membrane targeting? Perhaps the authors could clarify these aspects of the essay.

2. Using toeprinting and in vitro translation assays, the authors demonstrate that *C. kluyveri* CliM stalls ribosomes at two adjacent codons during elongation. In contrast to the *C. kluyveri* homolog, *C. difficile* CliM stalls at a single site corresponding to a termination event, with a stop codon positioned in the A-site. Toeprinting and biochemical analyses confirm that ribosomes reach the stop codon but fail to undergo peptidyl-tRNA hydrolysis, indicating arrest during translation termination.

A concern with these assays is that the differences observed between species may be due to limitations in toeprinting experiments to unambiguously define the stall site, caused by reverse transcriptase pausing or by RNA adopting different structures. Is that a possibility given the way the analysis was performed in this study?

3. The authors used *C. difficile* CliM to create a stalled ribosome and to study it using cryo-EM and single-particle analysis. The fact that *C. difficile* CliM stalls at a single site with the Phe76 codon in the P-site and a stop codon in the A-site makes

this an ideal sample for this analysis, rather than using a ribosome stalled with the *C. kluyveri* CliM that stalls at multiple sites. Three ribosomal states were resolved. All of them contained the P-tRNA-Phe linked to the NC. The three classes contain either an A-tRNA (the smallest class) or an empty A site or a bound release factor in the A-site, confirming that arrest occurs after RF binding but prior to peptide release. It is proposed that the A-tRNA bound state contains tRNA<sup>Tyr</sup>, which normally decodes UAC and UAU codons and has miscoded the UAA codon. Therefore, the most relevant class is the one bound to the RF and confirms that arrest occurs after RF binding but prior to peptide release. Structural analysis shows that CliM engages in extensive stacking, hydrogen-bonding, and hydrophobic interactions with 23S rRNA throughout the NPET. Many of these contacts involve residues identified as critical in the mutational scan, providing strong structure–function correlation. The authors demonstrate that CliM also makes specific interactions with the  $\beta$ -hairpin of uL22. Deletion of the uL22 tunnel loop abolishes arrest *in vivo*, whereas analogous deletions in uL4 or uL23 do not, establishing uL22 as a key structural determinant of CliM-mediated stalling. Comparison with accommodated release factor structures reveals that the penultimate CliM residue sterically blocks GGQ-loop accommodation at the PTC. Mutational analysis shows that reducing side-chain volume weakens or abolishes arrest, while larger residues preserve stalling, directly linking steric occlusion to arrest efficiency and stall-site position.

The structural analysis is excellent, and the cryo-EM maps are of high quality and resolution (~2.4 Å), specifically the density representing the nascent peptide. This is important because the mechanistic proposal of how the assembly is implemented requires the accurate positioning of key residues in the NC, and also nucleotides and r-proteins in the NPET. In particular, the claim that the position of the GGQ-loop in domain III of the RF, typically extending into the PTC, is displaced away by 3-4 Å. This is shown in Figure 7 with the molecular model, but the figure should also include a display of the relevant densities of the map for this region to support the accurate positioning of the model and ultimately the stated conclusion. Other than that, most of the conclusions derived from the structure are also validated with deletions and mutational assays, such as the involvement of uL22 in the stalling mechanism versus the requirement of, interactions with uL4 or uL23 that seem to be simply generic tunnel interactions.

Overall, I consider this manuscript very strong, and I support its publication after the authors address my concerns and comments described below.

Reviewer #2

(Remarks to the Author)

This manuscript presents a comprehensive and mechanistically insightful study of the arrest peptide CliM, establishing it as a functional ribosome stalling factor that senses YidC insertase activity. By integrating genetic reporter assays, *in vitro* translation, toeprinting, deep mutational scanning, high-resolution cryo-EM, and molecular dynamics simulations, the authors provide a coherent and largely convincing model explaining how CliM induces translational arrest during both elongation and termination. Overall, the study addresses a clearly defined and biologically relevant question, significantly expands the repertoire of known arrest peptides, and offers conceptual advances in our understanding of nascent chain-mediated translational control.

Major Concerns

1. The authors' main conclusion is that Leu75 prevents accommodation of either the GGQ motif of the release factor or the aminoacyl moiety of the A-site tRNA. The proposed rationale is that the helical structure of CliM constrains the position of Leu75, preventing it from undergoing the conformational rearrangement required for accommodation. However, a critical piece of evidence that is currently missing is a clear demonstration of how the CliM helix mechanically restricts the mobility of Leu75, especially given that Leu75 is already spatially distant from the CliM helix in the structure. Moreover, mutation of Leu75 to Gly results in +1 site stalling, indicating that this region retains a certain degree of conformational flexibility. Analogous to ErmDL-mediated arrest, which requires the additional presence of a macrolide antibiotic bound within the NPET to induce stalling, it remains unclear whether CliM-induced stalling at Leu75 is entirely dependent on the upstream helical elements. This issue could potentially be addressed by a more in-depth analysis integrating the deep mutational scanning data.

Minor Comments

1. It is recommended to include an additional table that integrates the deep mutational scanning data with structure-based interaction analysis, which would facilitate a clearer assessment of the consistency between the structural information and the mutational effects.  
2. The conformation of the RF GGQ loop in Figure 7 is critical to the proposed mechanism, and the corresponding cryo-EM map for this region should be shown to support the authors' conclusions.

Version 1:

Reviewer comments:

Reviewer #1

(Remarks to the Author)

I appreciate the authors addressing my concerns about the original submission and providing a revised version with the necessary changes. Specifically, the additional sentences discussing the results in Figure 1b, which show the beta-galactosidase assay data, and the revision of Figure 7. I think this is now an outstanding paper with extremely solid data

supporting all the conclusions. I support the publication in Nature Communications in the present form.

Reviewer #2

(Remarks to the Author)

The authors have nicely revised their manuscript and I have no further comments and fully support the publication of this work.

**Open Access** This Peer Review File is licensed under a Creative Commons Attribution 4.0 International License, which permits use, sharing, adaptation, distribution and reproduction in any medium or format, as long as you give appropriate credit to the original author(s) and the source, provide a link to the Creative Commons license, and indicate if changes were made.

In cases where reviewers are anonymous, credit should be given to 'Anonymous Referee' and the source.

The images or other third party material in this Peer Review File are included in the article's Creative Commons license, unless indicated otherwise in a credit line to the material. If material is not included in the article's Creative Commons license and your intended use is not permitted by statutory regulation or exceeds the permitted use, you will need to obtain permission directly from the copyright holder.

To view a copy of this license, visit <https://creativecommons.org/licenses/by/4.0/>

The reviewers' comments are shown in **bold**, and our point-by-point responses are presented in *Italics*.

## **Reviewer's Comments:**

### **Reviewer #1 (Remarks to the Author)**

**The manuscript reports a comprehensive analysis, using structural, biochemical, and mutational approaches, of the stalling mechanisms of the CliM stalling peptide. CliM is a membrane-insertion–sensing arrest peptide that couples YidC activity to feedback regulation of yidC expression. YidC is a membrane protein insertase in bacteria that helps newly synthesized membrane proteins insert into, and fold within, the lipid bilayer. As I described below, the study is strong with almost every conclusion supported by two or more experimental approaches. I just have a few small comments and suggestions regarding experiments in Fig 1, toeprinting experiments in Fig 2, and the cryo-EM section. I am describing these concerns below in the context of the specific experiments.**

**1. The authors demonstrate that CliM is a bona fide YidC-monitoring arrest peptide that regulates downstream yidC2 expression in response to membrane insertase activity. Using reporter assays in *B. subtilis*, they show that inhibition of CliM membrane insertion enhances yidC2 expression in an arrest-dependent manner, while successful insertion releases arrest. mRNA secondary structure analysis reveals that a stem–loop downstream of cliM mediates this regulation by coupling ribosome stalling to yidC2 translation. In Figure 1, the authors validate the proposed regulatory model in which CliM functions as a YidC activity sensor. Using spoIIIJ<sup>+</sup> (wild-type YidC1) and ΔspoIIIJ backgrounds as readouts of membrane-insertion capacity, the authors show that loss of SpoIIIJ selectively induces yidC2 expression in an arrest-dependent manner (Fig. 1b), while efficient insertion in the spoIIIJ<sup>+</sup> background relieves CliM stalling (Fig. 1c). Arrest-deficient CliM mutants abolish yidC2 induction even when SpoIIIJ is absent, demonstrating that translational stalling, rather than SpoIIIJ deletion per se, drives the response. Dissection of the downstream mRNA stem–loop (Fig. 1d) further shows how ribosome stalling is transduced into increased yidC2 translation, completing the regulatory circuit. Together, these experiments convincingly establish that CliM couples YidC activity to feedback regulation of yidC2 expression. These are the main experiments in the paper to validate the YidC2 regulatory model.**

**While these results support the proposed model, I would have expected a bigger difference in beta-galactose activity for the wild type construct between spoIIIJ<sup>+</sup> and ΔspoIIIJ in Fig 1b. Why does the wt construct in the spoIIIJ<sup>+</sup> produce so much signal if, in principle, there should be efficient CliM insertion, consequent arrest release, and thus low yidC2 expression? Also, how do the authors know that the key arrest-deficient mutations are solely affecting arrest and they are not altering membrane targeting? Perhaps the authors could clarify these aspects of the essay.**

*The relatively high basal expression of the downstream gene in the SpoIIIJ<sup>+</sup> strain is likely attributable to incomplete release of CliM-mediated arrest, even in the presence of SpoIIIJ. This interpretation is supported by the marked reduction in downstream gene expression observed in the arrest-deficient (KWm) mutant (Fig. 1b), as well as by the lower b-*

galactosidase activity of the WT variant relative to KWm in the Ck\_cliM-lacZ arrest reporter under SpoIIIJ-proficient conditions (Fig. 1c).

*We consider two possible explanations for the incomplete arrest release. First, CliM may not be efficiently inserted into the membrane by B. subtilis SpoIIIJ. Alternatively, although membrane insertion by SpoIIIJ may occur efficiently, it may not fully relieve translational arrest. In either case, these effects likely arise from heterologous expression of Clostridium CliM in B. subtilis.*

*Although the use of a heterologous expression system may partially obscure the native physiological behavior of CliM, we believe that the data are nevertheless sufficient to support our overall conclusions. These possibilities had already been discussed in the main text in relation to the results shown in Fig. 1c. We have now added a statement indicating that a similar interpretation also applies to the results shown in Fig. 1b (as underlined below).*

*“The lower activity of the WT reporter compared with the arrest-deficient mutant suggests that partial arrest persists even with the TM region, likely because B. subtilis SpoIIIJ does not efficiently insert heterologously expressed Ck CliM or fails to fully release arrest upon membrane insertion. **This notion may also account for the higher yidC'-lacZ induction observed for the WT reporter relative to the arrest-deficient mutant (Fig. 1b).**”*

*Because Figs. 1b and 1c provide complementary data, we believe that this revision improves the balance and clarity of the presentation.*

*We cannot formally exclude the possibility that the arrest-deficient mutations affect membrane targeting. However, our conclusion that arrest is essential for downstream gene expression is supported by experiments using TM-deleted CliM variants, in which membrane targeting is inherently impaired and thus potential effects of the arrest-deficient mutations on membrane targeting do not need to be considered. Under these conditions, the arrest-deficient mutation markedly reduced induction of the downstream gene (Fig. 1b; DTM vs DTM/KWm), supporting sufficiently our conclusion that arrest plays an essential role in downstream gene induction.*

**2. Using toeprinting and in vitro translation assays, the authors demonstrate that C. kluveri CliM stalls ribosomes at two adjacent codons during elongation. In contrast to the C. kluveri homolog, C. difficile CliM stalls at a single site corresponding to a termination event, with a stop codon positioned in the A-site. Toeprinting and biochemical analyses confirm that ribosomes reach the stop codon but fail to undergo peptidyl-tRNA hydrolysis, indicating arrest during translation termination.**

**A concern with these assays is that the differences observed between species may be due to limitations in toeprinting experiments to unambiguously define the stall site, caused by reverse transcriptase pausing or by RNA adopting different structures. Is that a possibility given the way the analysis was performed in this study?**

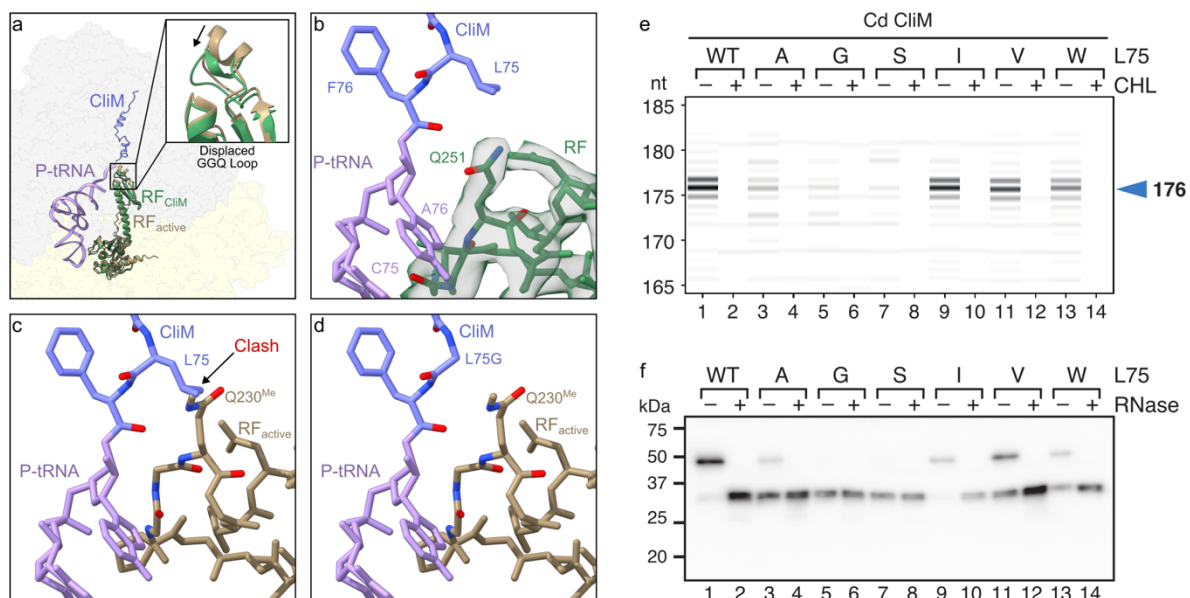
*Although reverse transcription can be prematurely terminated due to RNA secondary structures, such signals are also observed in toeprint assays performed with arrest-deficient mutants (KWm) or in the presence of the translation inhibitor chloramphenicol. By including these negative controls, we are able to distinguish translation arrest-dependent toeprint*

*signals from reverse transcription stops caused by RNA structure. Our data were interpreted with these controls. Therefore, it is unlikely that the differences in stalling sites observed between the two CliM homologs arise from the RNA secondary structure.*

**3. The authors used *C. difficile* CliM to create a stalled ribosome and to study it using cryo-EM and single-particle analysis. The fact that *C. difficile* CliM stalls at a single site with the Phe76 codon in the P-site and a stop codon in the A-site makes this an ideal sample for this analysis, rather than using a ribosome stalled with the *C. kluyveri* CliM that stalls at multiple sites. Three ribosomal states were resolved. All of them contained the P-tRNA-Phe linked to the NC. The three classes contain either an A-tRNA (the smallest class) or an empty A site or a bound release factor in the A-site, confirming that arrest occurs after RF binding but prior to peptide release. It is proposed that the A-tRNA bound state contains tRNA<sup>Tyr</sup>, which normally decodes UAC and UAU codons and has miscoded the UAA codon. Therefore, the most relevant class is the one bound to the RF and confirms that arrest occurs after RF binding but prior to peptide release. Structural analysis shows that CliM engages in extensive stacking, hydrogen-bonding, and hydrophobic interactions with 23S rRNA throughout the NPET. Many of these contacts involve residues identified as critical in the mutational scan, providing strong structure–function correlation. The authors demonstrate that CliM also makes specific interactions with the  $\beta$ -hairpin of uL22. Deletion of the uL22 tunnel loop abolishes arrest *in vivo*, whereas analogous deletions in uL4 or uL23 do not, establishing uL22 as a key structural determinant of CliM-mediated stalling. Comparison with accommodated release factor structures reveals that the penultimate CliM residue sterically blocks GGQ-loop accommodation at the PTC. Mutational analysis shows that reducing side-chain volume weakens or abolishes arrest, while larger residues preserve stalling, directly linking steric occlusion to arrest efficiency and stall-site position.**

**The structural analysis is excellent, and the cryo-EM maps are of high quality and resolution (~2.4 Å), specifically the density representing the nascent peptide. This is important because the mechanistic proposal of how the assembly is implemented requires the accurate positioning of key residues in the NC, and also nucleotides and r-proteins in the NPET. In particular, the claim that the position of the GGQ-loop in domain III of the RF, typically extending into the PTC, is displaced away by 3-4 Å. This is shown in Figure 7 with the molecular model, but the figure should also include a display of the relevant densities of the map for this region to support the accurate positioning of the model and ultimately the stated conclusion.**

*The density for the GGQ loop of the RF is shown in ED Fig 2, however, we have now revised Figure 7 panel b to also show the density for the GGQ loop there too as requested.*



Other than that, most of the conclusions derived from the structure are also validated with deletions and mutational assays, such as the involvement of uL22 in the stalling mechanism versus the requirement of, interactions with uL4 or uL23 that seem to be simply generic tunnel interactions. Overall, I consider this manuscript very strong, and I support its publication after the authors address my concerns and comments described below.

## Reviewer #2 (Remarks to the Author)

This manuscript presents a comprehensive and mechanistically insightful study of the arrest peptide CliM, establishing it as a functional ribosome stalling factor that senses YidC insertase activity. By integrating genetic reporter assays, *in vitro* translation, toeprinting, deep mutational scanning, high-resolution cryo-EM, and molecular dynamics simulations, the authors provide a coherent and largely convincing model explaining how CliM induces translational arrest during both elongation and termination. Overall, the study addresses a clearly defined and biologically relevant question, significantly expands the repertoire of known arrest peptides, and offers conceptual advances in our understanding of nascent chain-mediated translational control.

### Major Concerns

1. The authors' main conclusion is that Leu75 prevents accommodation of either the GGQ motif of the release factor or the aminoacyl moiety of the A-site tRNA. The proposed rationale is that the helical structure of CliM constrains the position of Leu75, preventing it from undergoing the conformational rearrangement required for accommodation. However, a critical piece of evidence that is currently missing is a clear demonstration of how the CliM helix mechanically restricts the mobility of Leu75, especially given that Leu75 is already spatially distant from the CliM helix in the structure. Moreover, mutation of Leu75 to Gly results in +1 site stalling, indicating that this region retains a certain degree of conformational flexibility. Analogous to ErmDL-mediated arrest, which requires the additional presence of a macrolide antibiotic bound

**within the NPET to induce stalling, it remains unclear whether CliM-induced stalling at Leu75 is entirely dependent on the upstream helical elements. This issue could potentially be addressed by a more in-depth analysis integrating the deep mutational scanning data.**

*The basis for the proposal that the helix mechanically restricts the mobility of Leu75 comes primarily from the molecular dynamics simulations that show that when the helix is in place, there is relatively little mobility of Leu and all accessible conformations would overlap with the RF (Fig. 8a, WT), however, once the helix is unwound the nascent chain naturally has more degrees of freedom. This hypothesis is supported by the mutagenesis data showing that proline substitutions that disrupt helix formation also lead to relief of stalling, which necessitates the movement of Leu75 out of the A-site pocket.*

*The suggestion from the reviewer that the mutation of Leu75 to Gly leads to stalling in the +1 position shows that the region retains a certain degree of flexibility, may have arisen from a misunderstanding since the Leu75 to Gly mutation only leads to +1 stalling when the stop codon is mutated to lysine (K77), as was used in the DMS analysis, and therefore does not occur in the natural Cd CliM staller that was used for the cryo-EM analysis. Moreover, even if we consider that stalling at the +1 position does lead to incorporation of another amino acid into the nascent chain, we do not know whether the mechanism of stalling at the +1 site is similar to that proposed here for CliM i.e. whether helix formation is actually required for stalling at the +1 site. Nevertheless, we cannot rule out that the PTC retains some plasticity such that the additional incorporation of another amino acid is possible, however, further work would be needed to address this hypothesis.*

### **Minor Comments**

**1. It is recommended to include an additional table that integrates the deep mutational scanning data with structure-based interaction analysis, which would facilitate a clearer assessment of the consistency between the structural information and the mutational effects.**

*We have now added a new Supplementary Fig. 4 that compares the deep mutational scanning data directly with interaction analysis from the cryo-EM structure of the CliM-SRC.*

**2. The conformation of the RF GGQ loop in Figure 7 is critical to the proposed mechanism, and the corresponding cryo-EM map for this region should be shown to support the authors' conclusions.**

*The density for the GGQ loop of the RF is shown in ED Fig 2, however, we have now revised figure 7b to also show the density for the GGQ loop there too, as also requested by Reviewer #1 (see response above with inserted revised Figure 7).*

## Description of Additional Supplementary Files

**File name: Supplementary Movie 1**

**Description:** Cryo-EM map of ClIM-SRC stalling at the stop codon of ClIM, including a section that reveals the quality of the density (transparent surface) for the nascent chain (blue), P-tRNA (purple) and the release factor (RF, green) together with the molecular model. The final part of the video shows an overlay of an active RF (PDB ID 9MTP<sup>28</sup>) against the RF from the ClIM-SRC, which illustrates an overlap of Q230 of the active RF with the penultimate residue from ClIM. This clash results in a displaced GGQ loop of the RF in ClIM.

## Supplementary Information

For

### **Diverse mechanisms of translation arrest by a Clostridia ribosome stalling peptide CliM**

Mayu Yoshida<sup>1,\*</sup>, Felix Gersteuer<sup>2,\*</sup>, Ole Berendes<sup>3</sup>, Keigo Fujiwara<sup>1,4</sup>, Haaris A. Safdari<sup>2</sup>, Helge Paternoga<sup>2</sup>, Hiraku Takada<sup>1,5</sup>, Nozomu Obana<sup>6,7</sup>, Helmut Grubmüller<sup>3</sup>, Lars Bock<sup>3</sup>, Daniel N. Wilson<sup>2,#</sup>, Shinobu Chiba<sup>1,#</sup>

<sup>1</sup> Faculty of Life Sciences and Institute for Protein Dynamics, Kyoto Sangyo University, Kamigamo, Motoyama, Kita-ku, Kyoto 603-8555, Japan.

<sup>2</sup> Institute for Biochemistry and Molecular Biology, Martin-Luther-King-Platz 6, University of Hamburg, 20146 Hamburg, Germany.

<sup>3</sup> Department of Theoretical and Computational Biophysics, Max Planck Institute for Multidisciplinary Sciences, Göttingen, Germany

<sup>4</sup> Department of Gene Function and Phenomics, National Institute of Genetics, Mishima, Japan

<sup>5</sup> Biotechnology Research Center and Department of Biotechnology, Toyama Prefectural University, 5180 Kurokawa, Imizu, Toyama 939-0398, Japan

<sup>6</sup> Transborder Medical Research Center, Institute of Medicine, University of Tsukuba, Tsukuba, Japan

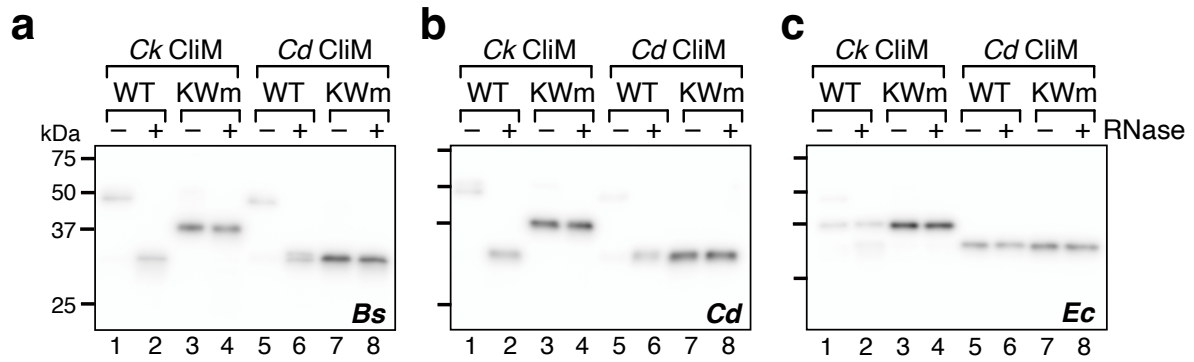
<sup>7</sup> Microbiology Research Center for Sustainability (MiCS), University of Tsukuba, Tsukuba, Japan

\* These authors contributed equally

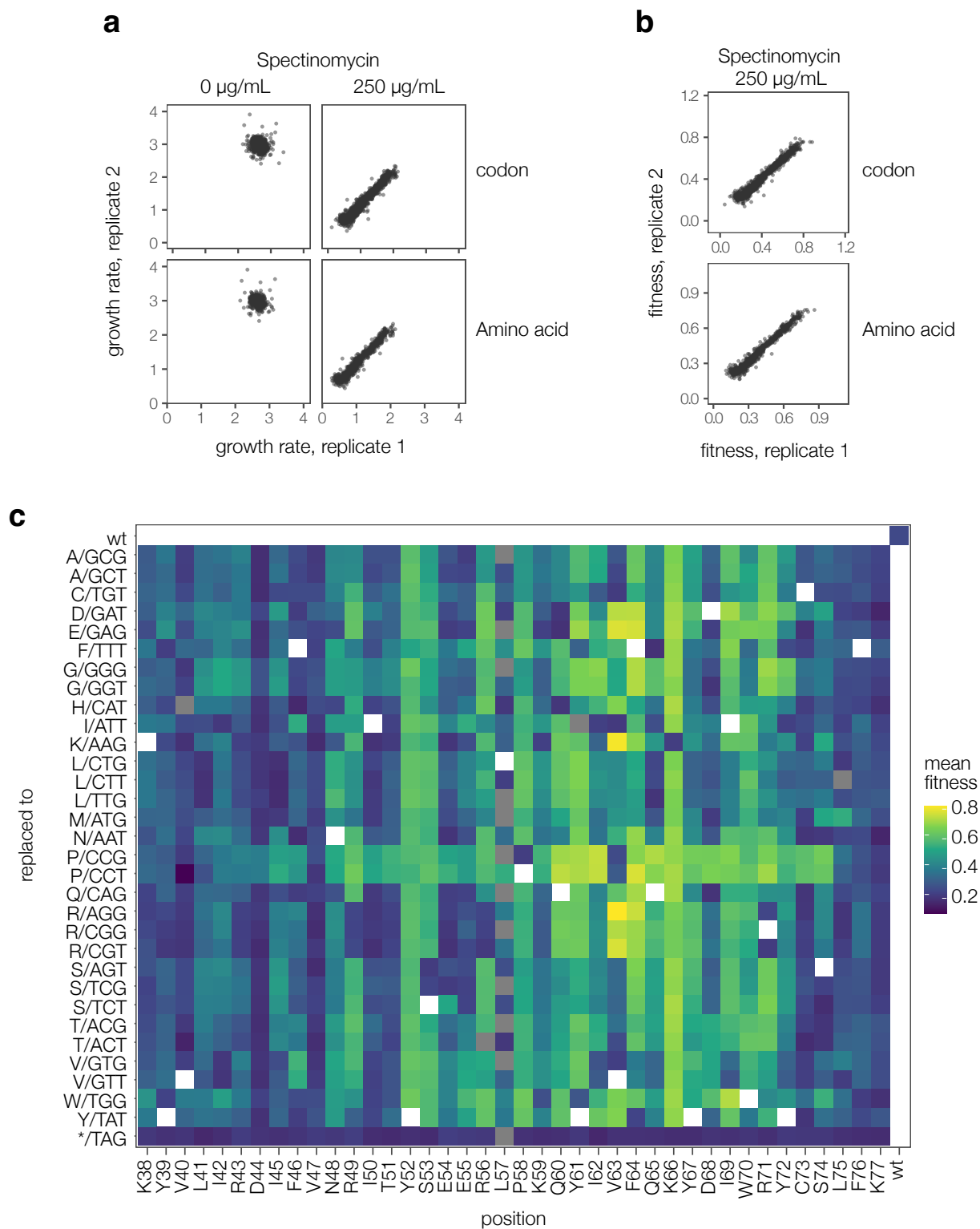
# Corresponding authors:

Prof Shinobu Chiba ([schiba@cc.kyoto-su.ac.jp](mailto:schiba@cc.kyoto-su.ac.jp))

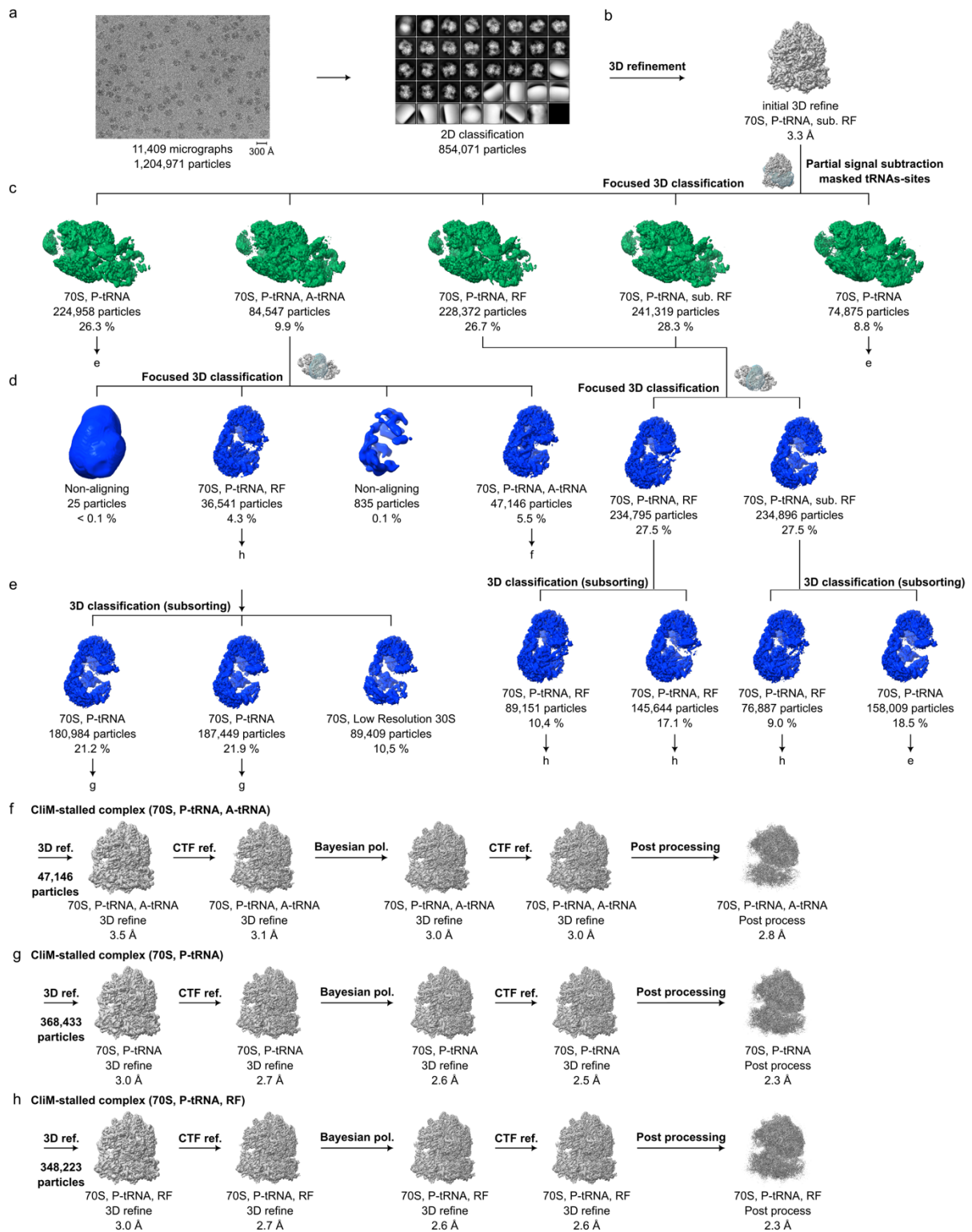
Prof Daniel N. Wilson ([Daniel.wilson@uni-hamburg.de](mailto:Daniel.wilson@uni-hamburg.de))



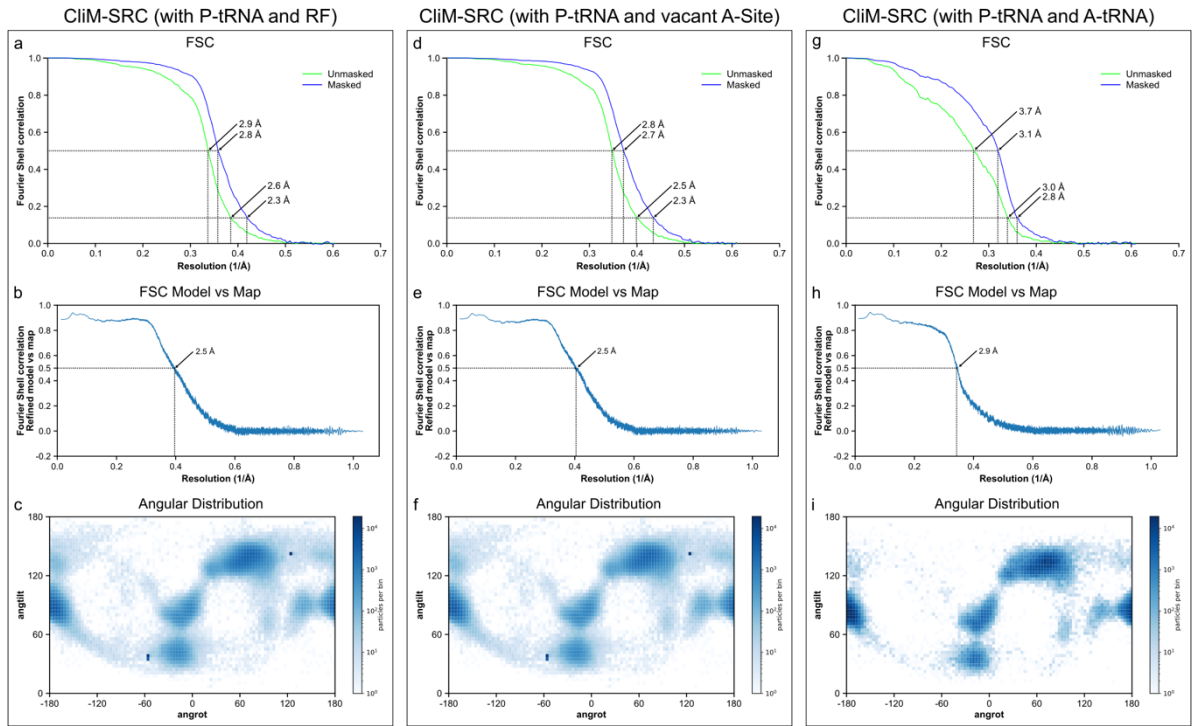
**Supplementary Fig. 1: Ck and Cd CliM arrest Bs and Cd ribosomes.** a-c Western blot analysis of the in vitro translation products of Ck and Cd CliM. WT or KWm mutant derivatives of the *gfp-cliM-myc-lacZ $\alpha$*  translational fusion reporters were translated in the Bs PURE (a), Cd PURE (b), or Ec PURE (c). The products were separated in neutral-pH gels and immunoblotted using anti-GFP antibody. Samples treated with RNase A (+) were analyzed alongside untreated samples (-) to distinguish peptidyl-tRNA from full-length hydrolyzed products. Molecular size markers (kDa) are shown on the left. Western blotting was independently repeated at least twice to ensure reproducibility. Source data are provided as a Source Data file.



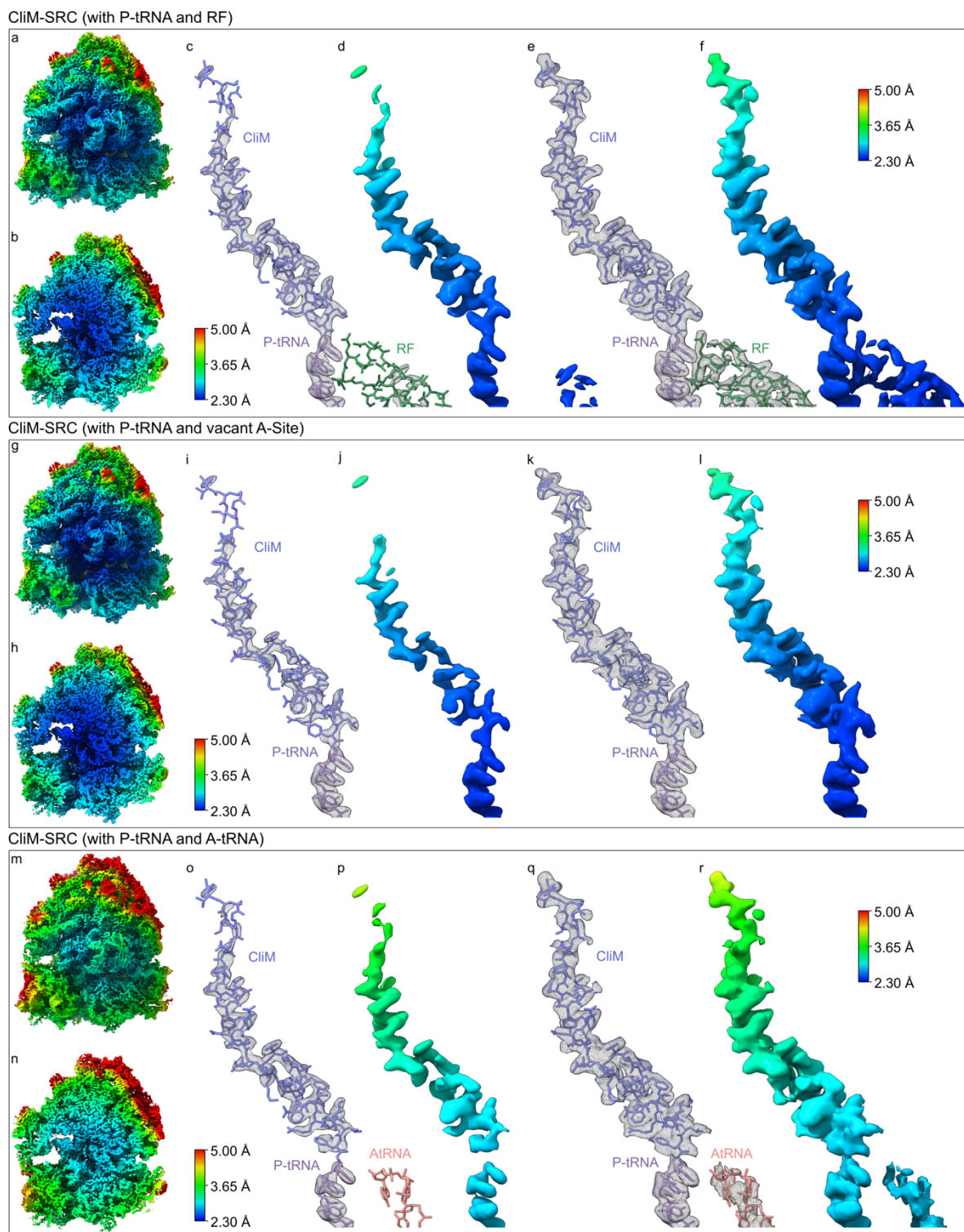
**Supplementary Fig. 2: Reproducibility of Deep mutational scanning.** (a-b) Scatter plots of growth rates (a) and fitness values (b) of each variant are shown at the codon level (upper) and at the amino acid level (lower), where amino acid-level values were obtained by averaging synonymous codon variants. In each plot, biological replicate 1 is shown on the x-axis and biological replicate 2 on the y-axis, demonstrating reproducibility across replicates. (c) The heatmap shows the relative fitness of each variant at the codon level, calculated as the mean of two biological replicates (related to Fig. 3), demonstrating that synonymous codon variants generally exhibit similar fitness values. Residue numbers and wild-type amino acids are indicated along the bottom, and substituted residues are shown along the left.



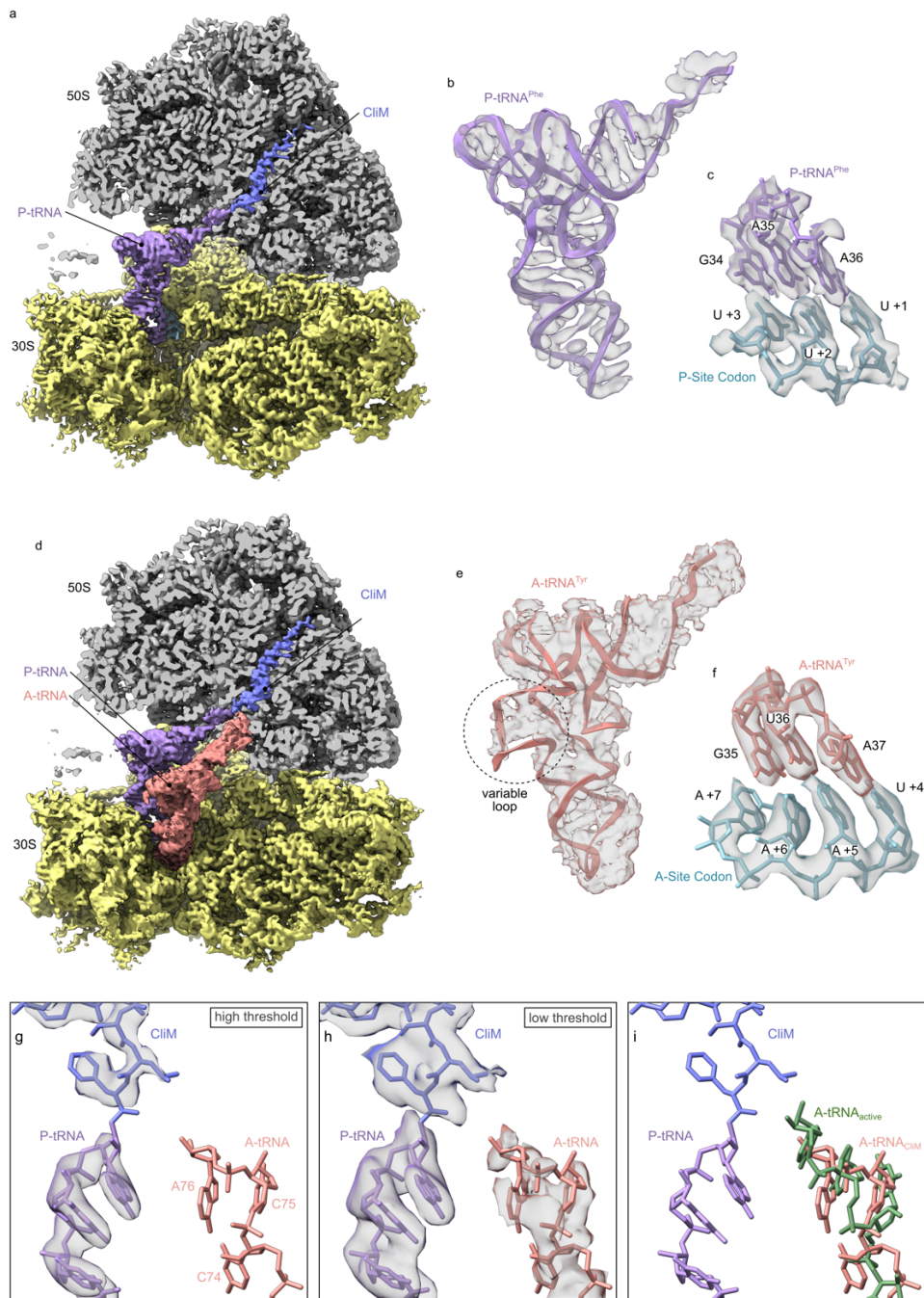
**Supplementary Fig. 3: *In silico* sorting scheme for CiIM.** (a) From 11,409 micrographs, 1,204,971 particles were picked and subjected to 2D classification resulting in 854,071 ribosome-like particles. Particles were (b) initially 3D-refined, then (c) subsorted into 5 classes using a mask around the tRNA binding sites. (d-e) The resulting classes with P-tRNA and vacant A-site, PtRNA and release factor as well as PtRNA and A-tRNA were further subsorted with a mask around the A-site until homogeneity was reached. The minor class with (f) both A- and P-tRNA density (5.5%) resulted in a final resolution (at FSC 0.143) of 2.8 Å. After combining of the respective particles, two major classes with (g) P-tRNA and vacant A-site (43.1%) as well as (h) P-tRNA and release factor (40.8%) resulted in a final resolution (at FSC 0.143) of 2.3 Å, respectively.



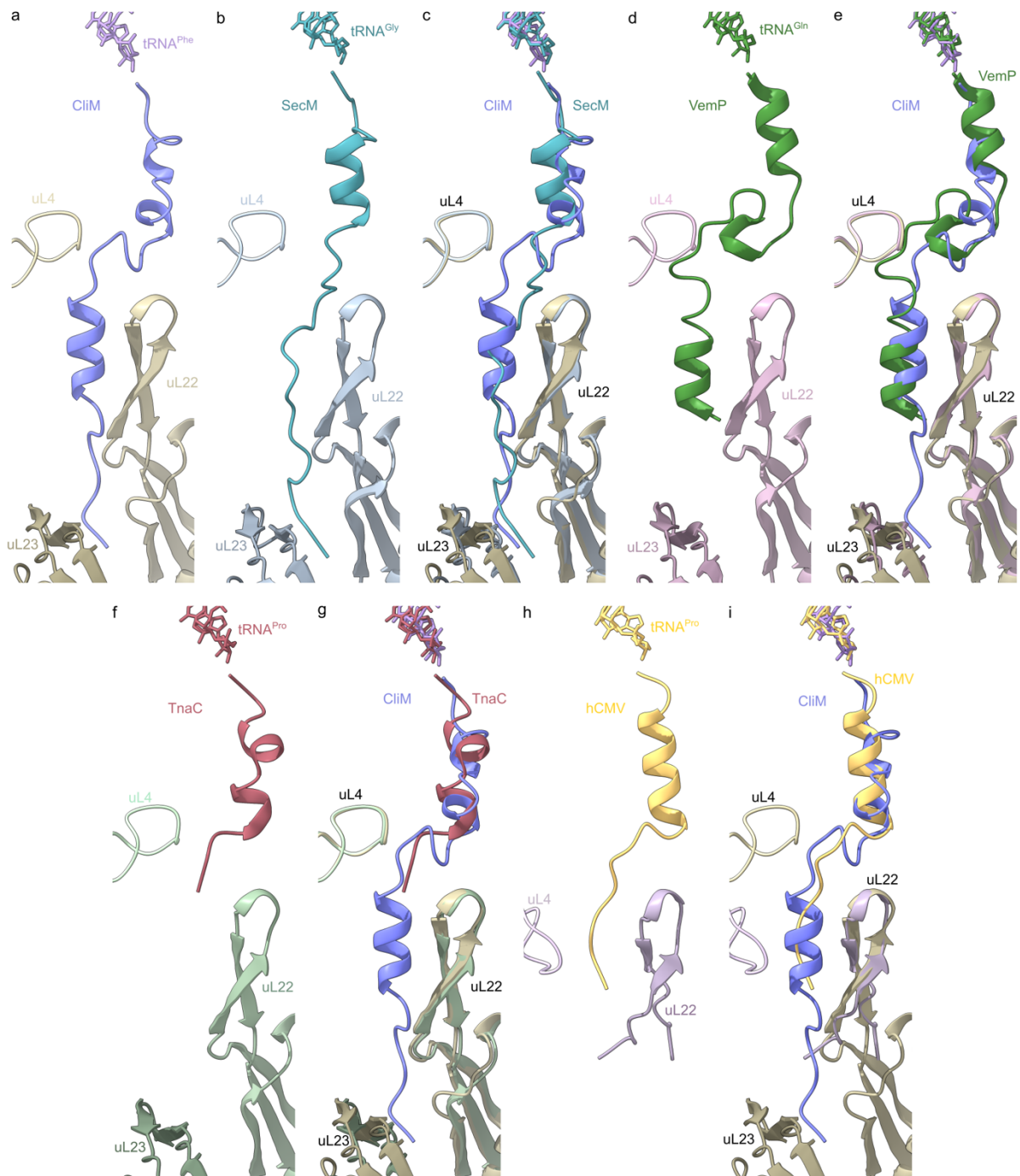
**Supplementary Fig. 4: Fourier Shell Correlation curves and angular distribution for CliM-SRC.** (a-c) Fourier shell correlation (FSC) curve of the (a) CliM-SRC containing P-tRNA and RF, (b) with P-tRNA and vacant A-site and (c) with P-tRNA and A-tRNA, with unmasked (green) and masked (blue) FSC curves plotted against the resolution ( $1/\text{\AA}$ ). (d-f) Refined model vs map FSC curve of the CliM-SRC from (a)-(c) plotted against the resolution ( $1/\text{\AA}$ ). (g-i) Angular distribution of particles used for 3D reconstruction from Relion for the CliM-SRC from (a)-(c). Particles are binned and logarithmical represented from white to blue.



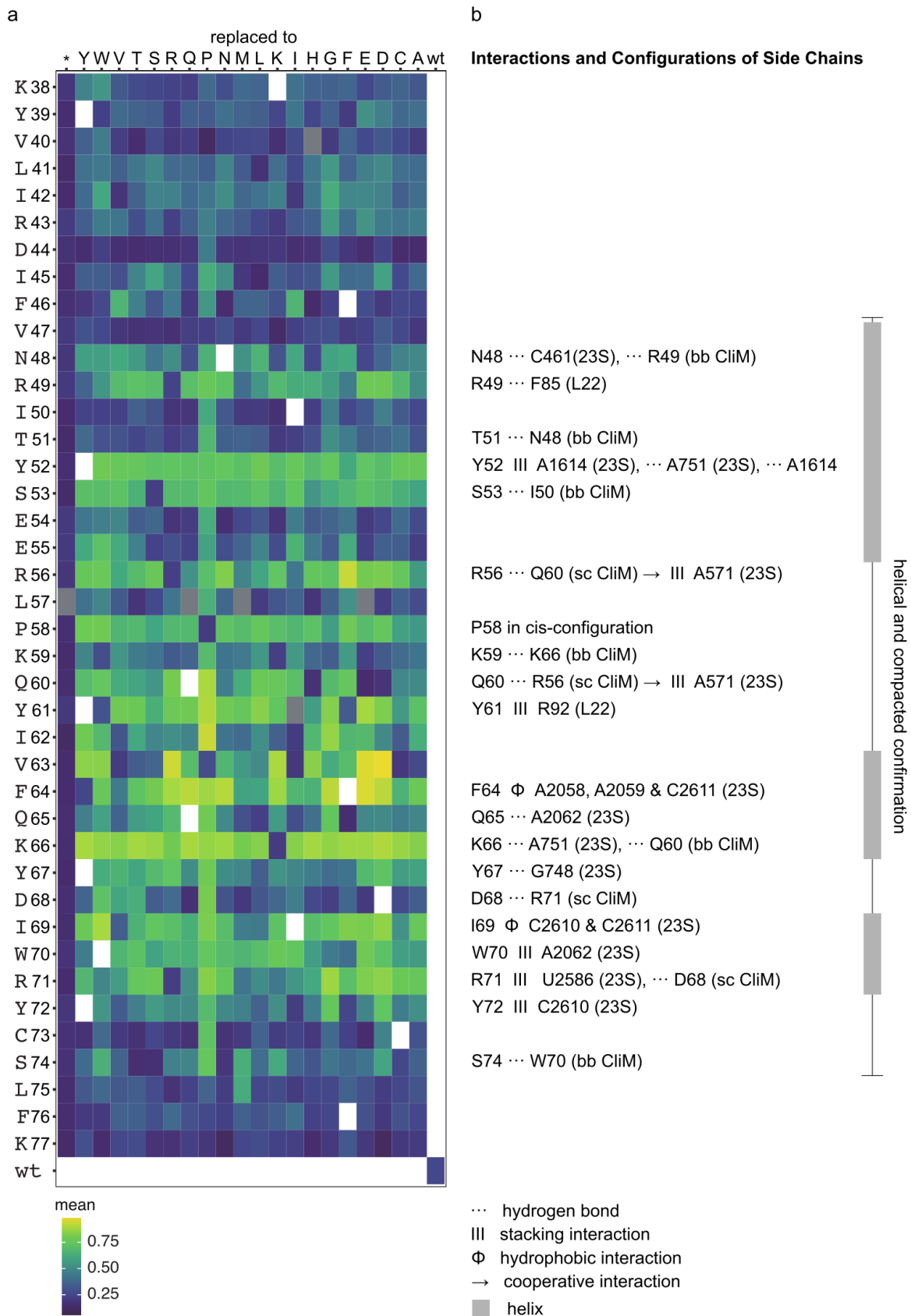
**Supplementary Fig. 5: Local resolution for the CliM-SRCs.** (a-r) Cryo-EM density for the 3D-refined map of the CliM-SRC with (a-f) P-tRNA and RF, (g-l) P-tRNA and vacant A-site, and (m-r) P-tRNA and A-tRNA, coloured according local resolution, or as transparent grey surface (c, e, i, k, o, q) with molecular model of the CliM-SRC taken from RF bound complex, and with A-tRNA (orange) in (o,q). In (a,g,m), overviews of the cryo-EM maps of the CliM-SRC are shown, whereas in (b,h,n), a transverse section reveals the core of the 50S subunit, including the ribosomal exit tunnel. In (e-f, k-l, q-r) the same representation is shown as in (c-d, i-j, o-p) but at a lower threshold.



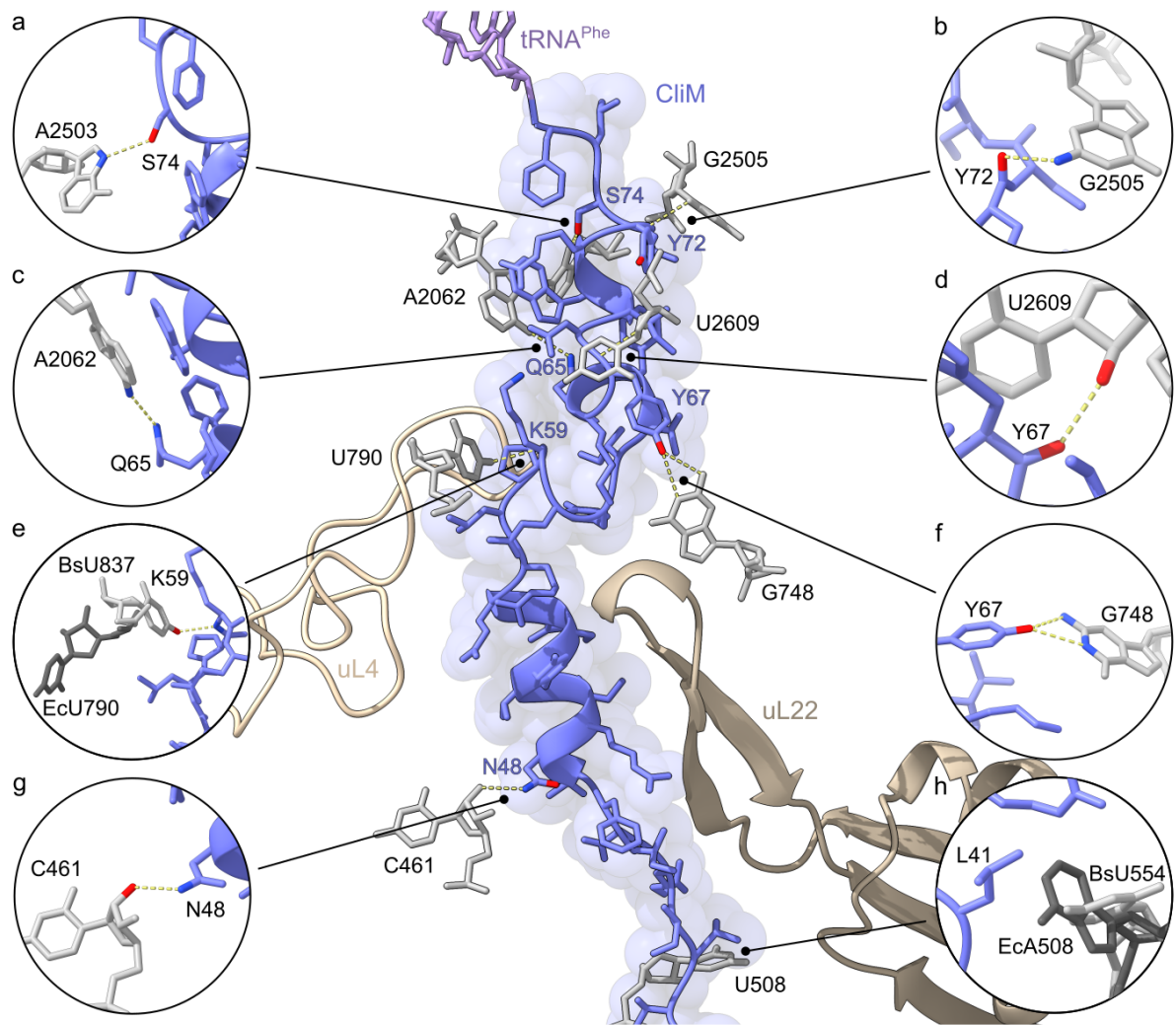
**Supplementary Fig. 6: Cryo-EM density for the P-tRNA and A-tRNA.** (a) Cryo-EM density for the 3D-refined map of the CliM-SRC (30S, yellow; 50S grey) with P-tRNA (purple) and vacant A-site, and transverse section of the 50S showing CliM nascent chain (blue) within the exit tunnel. (b-c) cryo-EM map density (transparent grey) for (b) the P-tRNA from (a) with fitted model for tRNA<sup>Phe</sup> (purple), and (c) anticodon of tRNA<sup>Phe</sup> in the P-site base-pairing with the UUU codon (positions +1 to +3) of the mRNA (green). (d) Cryo-EM density for the 3D-refined map of the CliM-SRC (30S, yellow; 50S grey) with P-tRNA (purple) and A-tRNA, and transverse section of the 50S showing CliM nascent chain (blue) within the exit tunnel. (e-f) cryo-EM map density (transparent grey) for (e) the A-tRNA from (d) with fitted model for tRNA<sup>Tyr</sup> (brown), and (f) anticodon of tRNA<sup>Tyr</sup> in the P-site base-pairing with the UAA stop codon (positions +4 to +6) of the mRNA (green). (g-i) View of the PTC of the (g-h) A-tRNA (rose) containing state of CliM (blue) that shows a flexible CCA-end of the A-tRNA by missing density at (g) high threshold, and (h) low threshold with noisy density, and no proper accommodation shown by the comparison with a (i) CCA-end of an properly accommodated tRNA (green) (PDB ID 8CVK)<sup>1</sup>, in the A-site of the PTC.



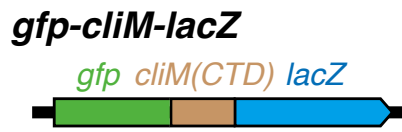
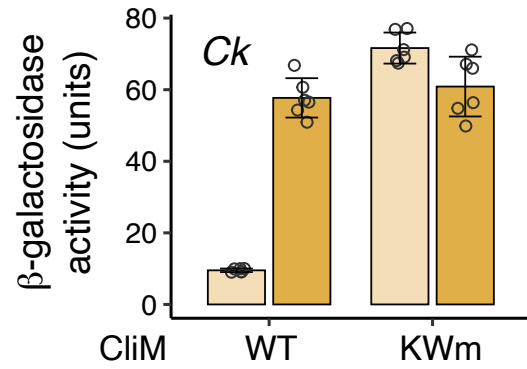
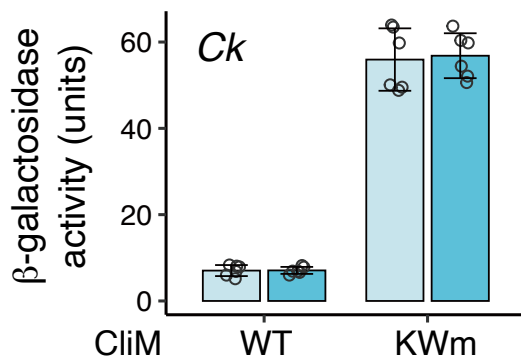
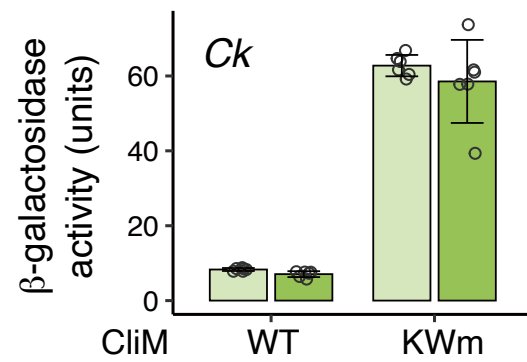
**Supplementary Fig. 7: Comparison of CliM with SecM, VemP and TnaC arrest peptides.** (a) CliM (blue) attached to the P-tRNA (lavender) in relation to uL4 (light gold), uL22 (gold) and uL23 (dark gold). (b) SecM (PDB ID 8QOA)<sup>2</sup> attached to the P-tRNA (teal) in relation to uL4 (light slate blue), uL22 (slate blue) and uL23 (dark slate blue). (c) Overlay (aligned on the basis of 23S rRNA) of (a) CliM and (b) SecM. (d) VemP (PDB ID 5NWX)<sup>3</sup> attached to the P-tRNA (green) in relation to uL4 (light rose), uL22 (rose) and uL23 (dark rose). (e) Overlay (aligned on the basis of 23S rRNA) (a) CliM and (d) VemP. (f) TnaC (PDB ID 7O19)<sup>4</sup> attached to the P-tRNA (red) in relation to uL4 (light mint), uL22 (mint) and uL23 (dark mint). (g) Overlay (aligned on the basis of 23S rRNA) of (a) CliM and (f) TnaC. (h) hCMV (PDB ID 5A8I)<sup>5</sup> attached to the P-tRNA (gold) in relation to uL4 (pink) and uL22 (purple). (i) Overlay (aligned on the basis of 23S rRNA) of (a) CliM and (h) hCMV.



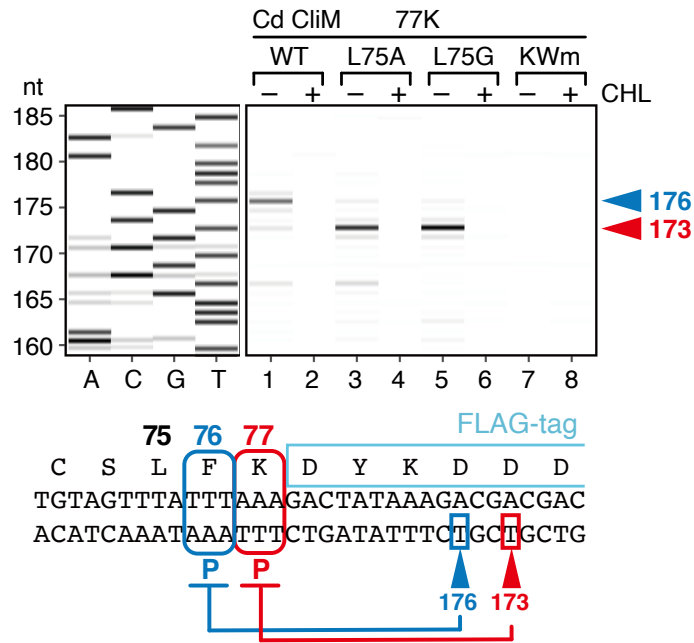
**Supplementary Fig. 8: Correlation between DMS-seq and cryo-EM data for CliM.** **a**, Heatmap from Fig 3c of relative fitness (mean of two biological replicate) of each CliM mutant compared with **b**, interactions of CliM sidechain observed in the cryo-EM structure of CliM-SRC. CliM secondary structure is also indicated.



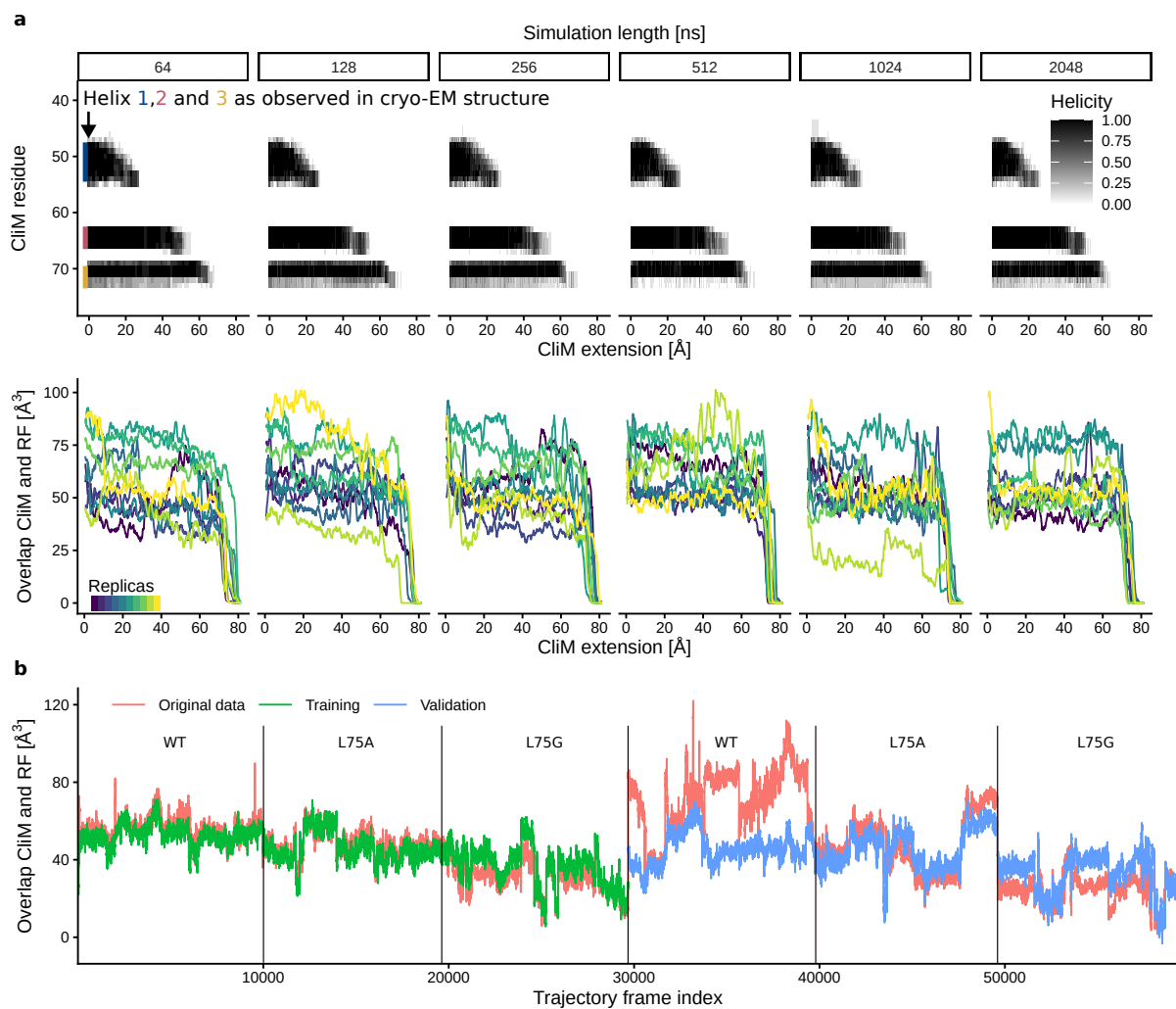
**Supplementary Fig. 9: Interaction of CliM with nucleotides of the 23S rRNA.** (a-h) The central panel shows the CliM nascent chain (blue) attached to the P-site tRNA (lavender) and ribosomal proteins uL4 (light gold) and uL22 (gold), with selected contacts with the 23S rRNA (grey) highlighted by individual panels. Dashed yellow lines indicated potential hydrogen bond interactions.

**a****b uL22****c uL4****d uL23**

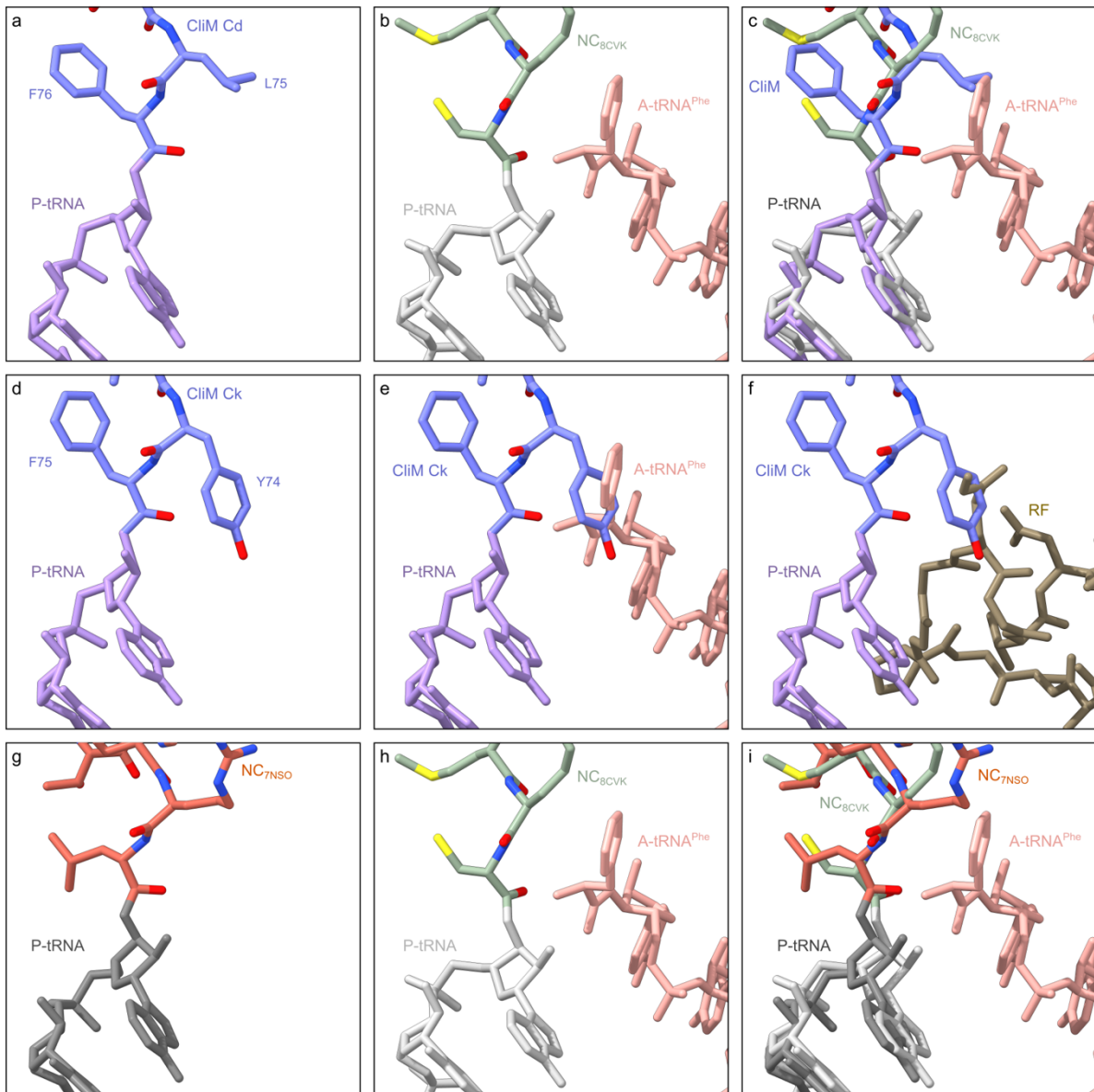
**Supplementary Fig. 10: Mutation in uL22 abolishes arrest by Ck CliM.** **a** Schematic representation of *gfp-cliM-lacZ* reporter. A gene fragment encoding the C-terminal domain (CTD) of Ck CliM was fused in-frame with *gfp* and *lacZ*. **b-d**  $\beta$ -galactosidase activity (mean  $\pm$  s.d., n=6, biologically independent cultures) of *B. subtilis* cells carrying WT or KWm derivatives of the *gfp-cliM-lacZ* reporter with (dark bars) or without (light bars) loop deletions in uL22 (b), uL4 (c), or uL23 (d). Source data are provided as a Source Data file.



**Supplementary Fig. 11: Flexible stalling site selection determined by local sequence context.** Toeprinting analysis of WT and Leu75 mutant derivatives of Cd CliM with substitution of the stop codon by Lys (77K). The reverse translation products were analyzed by capillary sequencer and signals were represented as a gel-style heatmap. In vitro translation was performed in the presence or absence of chloramphenicol (CHL). The toeprint length (nt) were calibrated against dideoxy sequencing (left). The estimated stalling sites (P-site codon) based on the toeprint length are shown with their codon numbers (bottom). Toeprinting analysis was independently repeated at least twice to ensure reproducibility. Source data are provided as a Source Data file.



**Supplementary Fig. 12: CliM dynamics during constant-velocity pulling MD simulations and cross-validation of functional mode analysis (FMA).** (a) Top panel: For different pulling simulation lengths, the time evolution of the helicity per residue is shown. Helicity is defined as the average of secondary structure states (1: Residue part of helix, 0: Residue not part of helix) over 10 independent simulation replicas. Colored bars in the leftmost panel show the secondary structure of the cryo-EM model. Bottom panel: Time evolution of the overlap volume between CliM and aligned RF for each simulation replica. (b) Comparison of measured overlap volume for frames of all unbiased MD simulation trajectories (WT and L75A, L75G mutants, red line) with overlap volume predicted from FMA (green for training, blue for validation).



**Supplementary Fig. 13: Comparison of CliM with accommodated A-tRNA.** (a) View of the PTC of the A-tRNA containing state of CliM (blue) attached to the P-tRNA (purple). (b) View of the PTC of a pre-attack state (PDB ID 8CVK)<sup>1</sup>, showing a tripeptidyl-NH-tRNA (green/light grey) at the P-site and a phenyl-NH-tRNA (rose) at the A-site. (c) Overlay of (a) and (b) (aligned on the basis of 23S rRNA) highlighting the incompatibility of CliM's penultimate residue Leu75 position and an accommodated aminoacyl-tRNA moiety in the A-site of the PTC. (d) In silico created CliM Ck (blue) mutated from CliM Cd attached to the P-tRNA (purple). (e-f) Overlay of (d) CliM Ck with (e) phenyl-NH-tRNA (rose) (PDB ID 8CVK)<sup>1</sup> and (f) release factor 1 (brown) (PDB ID 9MTP)<sup>6</sup> in the A-site, highlighting the incompatibility of proper accommodation into the A-site of the PTC for both with Tyr in the penultimate position of the CliM nascent peptide. (g) View of the PTC of stalled ErmDL peptide (red)(PDB ID 7NSO)<sup>7</sup> attached to the P-tRNA (dark grey). (h) Same panel as in (b). (i) Overlay of (g) and (h) (aligned of the basis of 23S rRNA) highlighting the similarity of ErmDL- and CliM-induced stalling by encroaching penultimate nascent peptide residues into the A-site that are incompatible with proper accommodation of an aminoacyl-tRNA moiety in the A-site of the PTC.

## Supplementary Table 1: Strain list

strain	plasmid	host	genotype
SCB4668	pCH2713	SCB3065	spoIIJ $\Omega$ kan, amyE::Ck_CliM-lacZ $\Omega$ cat
SCB4669	pCH2714	SCB3065	spoIIJ $\Omega$ kan, amyE::Ck_CliM(dTM)-lacZ $\Omega$ cat
SCB4670	pCH2715	SCB3065	spoIIJ $\Omega$ kan, amyE::Ck_CliM(K65A/W69A)-lacZ $\Omega$ cat
SCB4671	pCH2716	SCB3065	spoIIJ $\Omega$ kan, amyE::Ck_CliM(dTM/K65A/W69A)-lacZ $\Omega$ cat
SCB4676	pCH2713	SCB2969	AspoIIIJ::tet, amyE::Ck_CliM-lacZ $\Omega$ cat
SCB4677	pCH2714	SCB2969	AspoIIIJ::tet, amyE::Ck_CliM(dTM)-lacZ $\Omega$ cat
SCB4678	pCH2715	SCB2969	AspoIIIJ::tet, amyE::Ck_CliM(K65A/W69A)-lacZ $\Omega$ cat
SCB4679	pCH2716	SCB2969	AspoIIIJ::tet, amyE::Ck_CliM(dTM/K65A/W69A)-lacZ $\Omega$ cat
SCB4696	pCH2736	SCB3065	spoIIJ $\Omega$ kan, amyE::Ck_CliM-Dstem2-yidC2(1-6)-lacZ $\Omega$ cat
SCB4697	pCH2737	SCB3065	spoIIJ $\Omega$ kan, amyE::Ck_CliM(dTM)-Dstem2-yidC2(1-6)-lacZ $\Omega$ cat
SCB4698	pCH2738	SCB3065	spoIIJ $\Omega$ kan, amyE::Ck_CliM(K65A/W69A)-Dstem2-yidC2(1-6)-lacZ $\Omega$ cat
SCB4699	pCH2739	SCB3065	spoIIJ $\Omega$ kan, amyE::Ck_CliM(dTM/K65A/W69A)-Dstem2-yidC2(1-6)-lacZ $\Omega$ cat
SCB4700	pCH2736	SCB2969	AspoIIIJ::tet, amyE::Ck_CliM-Dstem2-yidC2(1-6)-lacZ $\Omega$ cat
SCB4701	pCH2737	SCB2969	AspoIIIJ::tet, amyE::Ck_CliM(dTM)-Dstem2-yidC2(1-6)-lacZ $\Omega$ cat
SCB4702	pCH2738	SCB2969	AspoIIIJ::tet, amyE::Ck_CliM(K65A/W69A)-Dstem2-yidC2(1-6)-lacZ $\Omega$ cat
SCB4703	pCH2739	SCB2969	AspoIIIJ::tet, amyE::Ck_CliM(dTM/K65A/W69A)-Dstem2-yidC2(1-6)-lacZ $\Omega$ cat
YSB117	pKIG1225	SCB2634	rplW(d65-69) $\Omega$ kan, amyE::PmifM-gfp-Ck_cliM-lacZ $\Omega$ cat
YSB118	pYS37	SCB2634	rplW(d65-69) $\Omega$ kan, amyE::PmifM-gfp-Ck_cliM(K65A W69A)-lacZ $\Omega$ cat
YSB119	pCH2675	SCB2613	rplW $\Omega$ kanWrplB, amyE::PmifM gfp-Cd_cliM(30-76)-R71CGG_L75TTA_77K-flag-lacZ $\Omega$ cat
YSB120	pCH2691	SCB2613	rplW $\Omega$ kanWrplB, amyE::PmifM gfp-Cd_cliM(30-76)-(K66A/W70A)-R71CGG_L75TTA_77K-flag-lacZ $\Omega$ cat
YSB121	pCH2675	SCB2942	rplD(d66-70) $\Omega$ kan, amyE::PmifM gfp-Cd_cliM(30-76)-R71CGG_L75TTA_77K-flag-lacZ $\Omega$ cat
YSB122	pCH2691	SCB2942	rplD(d66-70) $\Omega$ kan, amyE::PmifM gfp-Cd_cliM(30-76)-(K66A/W70A)-R71CGG_L75TTA_77K-flag-lacZ $\Omega$ cat
YSB123	pCH2675	SCB2634	rplW(d65-69) $\Omega$ kan, amyE::PmifM gfp-Cd_cliM(30-76)-R71CGG_L75TTA_77K-flag-lacZ $\Omega$ cat
YSB124	pCH2691	SCB2634	rplW(d65-69) $\Omega$ kan, amyE::PmifM gfp-Cd_cliM(30-76)-(K66A/W70A)-R71CGG_L75TTA_77K-flag-lacZ $\Omega$ cat
YSB125	pCH2675	SCB2656	rpsS $\Omega$ kan, amyE::PmifM gfp-Cd_cliM(30-76)-R71CGG_L75TTA_77K-flag-lacZ $\Omega$ cat
YSB126	pCH2691	SCB2656	rpsS $\Omega$ kan, amyE::PmifM gfp-Cd_cliM(30-76)-(K66A/W70A)-R71CGG_L75TTA_77K-flag-lacZ $\Omega$ cat
YSB127	pCH2675	SCB2917	rpsS $\Omega$ kanWrplV(d86-90), amyE::PmifM gfp-Cd_cliM(30-76)-R71CGG_L75TTA_77K-flag-lacZ $\Omega$ cat
YSB128	pCH2691	SCB2917	rpsS $\Omega$ kanWrplV(d86-90), amyE::PmifM gfp-Cd_cliM(30-76)-(K66A/W70A)-R71CGG_L75TTA_77K-flag-lacZ $\Omega$ cat
YSB129	pCH2675	PY79	amyE::PmifM gfp-Cd_cliM(30-76)-R71CGG_L75TTA_77K-flag-lacZ $\Omega$ cat
YSB130	pCH2691	PY79	amyE::PmifM gfp-Cd_cliM(30-76)-(K66A/W70A)-R71CGG_L75TTA_77K-flag-lacZ $\Omega$ cat
YSB41	pKIG1225	PY79	amyE::PmifM-gfp-Ck_cliM-lacZ $\Omega$ cat
YSB45	pYS37	PY79	amyE::PmifM-gfp-Ck_cliM(K65A W69A)-lacZ $\Omega$ cat
YSB65	pYS47	SCB3065	spoIIJ $\Omega$ kan, amyE::PmifM-Ck_cliM-Ck_YidC2(1-6aa)-lacZ $\Omega$ cat
YSB66	pYS50	SCB3065	spoIIJ $\Omega$ kan, amyE::PmifM-Ck_cliM(dTM)-Ck_YidC2(1-6aa)-lacZ $\Omega$ cat
YSB67	pYS49	SCB3065	spoIIJ $\Omega$ kan, amyE::PmifM-Ck_cliM(K65A W69A)-Ck_YidC2(1-6aa)-lacZ $\Omega$ cat
YSB68	pYS51	SCB3065	spoIIJ $\Omega$ kan, amyE::PmifM-Ck_cliM(dTM K65A K69A)-Ck_YidC2(1-6aa)-lacZ $\Omega$ cat
YSB69	pYS47	SCB2969	AspoIIIJ::tet, amyE::PmifM-Ck_cliM-Ck_YidC2(1-6aa)-lacZ $\Omega$ cat
YSB70	pYS50	SCB2969	AspoIIIJ::tet, amyE::PmifM-Ck_cliM(dTM)-Ck_YidC2(1-6aa)-lacZ $\Omega$ cat
YSB71	pYS49	SCB2969	AspoIIIJ::tet, amyE::PmifM-Ck_cliM(K65A W69A)-Ck_YidC2(1-6aa)-lacZ $\Omega$ cat
YSB72	pYS51	SCB2969	AspoIIIJ::tet, amyE::PmifM-Ck_cliM(dTM K65A K69A)-Ck_YidC2(1-6aa)-lacZ $\Omega$ cat
YSB81	pKIG1225	SCB2613	rplW $\Omega$ kanWrplB, amyE::PmifM-gfp-Ck_cliM-lacZ $\Omega$ cat
YSB82	pYS37	SCB2613	rplW $\Omega$ kanWrplB, amyE::PmifM-gfp-Ck_cliM(K65A W69A)-lacZ $\Omega$ cat
YSB83	pKIG1225	SCB2942	rplD(d66-70) $\Omega$ kan, amyE::PmifM-gfp-Ck_cliM-lacZ $\Omega$ cat
YSB84	pYS37	SCB2942	rplD(d66-70) $\Omega$ kan, amyE::PmifM-gfp-Ck_cliM(K65A W69A)-lacZ $\Omega$ cat
YSB85	pKIG1225	SCB2656	rpsS $\Omega$ kan, amyE::PmifM-gfp-Ck_cliM-lacZ $\Omega$ cat
YSB86	pYS37	SCB2656	rpsS $\Omega$ kan, amyE::PmifM-gfp-Ck_cliM(K65A W69A)-lacZ $\Omega$ cat
YSB87	pKIG1225	SCB2917	rpsS $\Omega$ kanWrplV(d86-90), amyE::PmifM-gfp-Ck_cliM-lacZ $\Omega$ cat
YSB88	pYS37	SCB2917	rpsS $\Omega$ kanWrplV(d86-90), amyE::PmifM-gfp-Ck_cliM(K65A W69A)-lacZ $\Omega$ cat

Supplementary Table 2. Plasmid construction

plasmid	primer fw1	primer rv1	template 1	primer fw2	primer rv2	template 2	primer fw3	primer rv3	template 3	ref
pCH2126										Sakiyama 2021
pCH2527	amyE-front-1w	pDG 1662-DspcR-fw	psK69	pDG 1662-DspcR-rv	FLAG_2-7-rv	psK69	FLAG-SpcR-fw	amyE-SpcR-rv	psK69	
pCH2612	flag-fw	gfp238-rv	pCH2627	gfp238-fw	Cdf1_KYX1W-K-flag-rv	pKIG1283				
pCH2674	CIM-R71CGG-L75TTA-FLAG-1w		pCH2612							
pCH2675	flag-fw	gfp238-rv	pCH2126	gfp238-fw	flag_2-7-rv	pCH2674				
pCH2691	Cd_CIM-repro-KWm-fw	Cd_CIM-KWm-rv	pCH2675							
pCH2713	CIM-LacZ nontGA fw	Ck non TGA LacZ rv	pYS48							
pCH2714	CIM-LacZ nontGA fw	Ck non TGA LacZ rv	pYS49							
pCH2715	CIM-LacZ nontGA fw	Ck non TGA LacZ rv	pYS50							
pCH2716	CIM-LacZ nontGA fw	Ck non TGA LacZ rv	pYS51							
pCH2730	Cd_CIM-RE-77STP-FL-fw	Cd_CIM_RE-S74-rv	pCH2675							
pCH2731	Cd_CIM-RE-L75A-77STP-FL-fw	Cd_CIM_RE-S74-rv	pCH2675							
pCH2732	Cd_CIM-RE-L75G-77STP-FL-fw	Cd_CIM_RE-S74-rv	pCH2675							
pCH2736	Ck_CIM-Dstem2-fw	Ck_CIM-Dstem2-rv	pCH2717							
pCH2737	Ck_CIM-Dstem2-fw	Ck_CIM-Dstem2-rv	pCH2718							
pCH2738	Ck_CIM-Dstem2-fw	Ck_CIM-Dstem2-rv	pCH2719							
pCH2739	Ck_CIM-Dstem2-fw	Ck_CIM-Dstem2-rv	pCH2720							
pCH2764	Cd_CIM-RE-76stp-FL-fw	Cd_CIM-C73-rv	pCH2730							
pCH2765	Cd_CIM-S74L-76stp-FL-fw	Cd_CIM-C73-rv	pCH2730							
pCH2767	Cd_CIM-S74G-76stp-FL-fw	Cd_CIM-C73-rv	pCH2730							
pCH2768	Cd_CIM-S74V-76stp-FL-fw	Cd_CIM-C73-rv	pCH2730							
pCH2774	Cd_CIM-RE-L75DKK-77STP-FL-fw	Cd_CIM_RE-S74-rv	pCH2730							
pCH2779	Cd_CIM-RE-L75S-77STP-FL-fw	Cd_CIM_RE-S74-rv	pCH2730							
pCH2780	Cd_CIM-RE-L75I-77STP-FL-fw	Cd_CIM_RE-S74-rv	pCH2730							
pCH2781	Cd_CIM-RE-L75V-77STP-FL-fw	Cd_CIM_RE-S74-rv	pCH2730							
pKIG 1225										
pKIG 1283	Cd_AP_wt fw	Cd_AP_wt rv	chrDNA of C. difficile 630	myc-lacZ-fw	gfp238-rv	psK69				Fujiwara 2024
pKIG 1284	Cd_AP_wt fw	Cd_AP_stp77A rv	chrDNA of C. difficile 630	myc-lacZ-rv	gfp238-rv	psK69				
pKIG 1285	Cd_AP_wt fw	Cd_AP_stp77K rv	chrDNA of C. difficile 630	myc-lacZ-fw	gfp238-rv	psK69				
pKIG 1288	amp121-128(TM62)	Cdf AP Q65 rv	pKIG 1283	Cdf AP K66A W70A fw	amp121-128(TM62) antisense	pKIG1283				
psK69										
pYS37	amp121-128(TM62)	uYrdC-Ob_klu-E64 rv	pKIG 1225							
pYS38	amp121-128(TM62)	Cd_AP_F76stp rv	pKIG 1283	myc24 fw	amp121-128(TM62) antisense	pKIG1225				
pYS39	amp121-128(TM62)	Cd_AP_F75stp rv	pKIG 1283	myc24 fw	amp121-128(TM62) antisense	pKIG1283				
pYS40	amp121-128(TM62)	Ck_AP_F76stp rv	pKIG 1225	myc24 fw	amp121-128(TM62) antisense	pKIG1225				
pYS41	amp121-128(TM62)	Ck_AP_F75stp rv	pKIG 1225	myc24 fw	amp121-128(TM62) antisense	pKIG1225				
pYS42	amp121-128(TM62)	Ck_AP_F74stp rv	pKIG 1225	myc24 fw	amp121-128(TM62) antisense	pKIG1225				
pYS47	C-kluyv-pCH746-fw	C-kluyv-pCH746 rv	uYrdC-Obst_kluyv (GeneArt Strings DNA Fragments)	lacZ_lba4-fw	Prn1fM-16nt 27rv	pCH746				
pYS49	amp121-128(TM62)	uYrdC-Ob_klu-E64 rv	pYS47	uYrdC_Ob_klu_K65A-W69A	amp121-128(TM62) antisense	pYS47				
pYS50	amp121-128(TM62)	C. kluyv dele_TM12-21 rv	pYS47	C. kluyv dele_TM12-21 fw	amp121-128(TM62) antisense	pYS47				
pYS51	amp121-128(TM62)	uYrdC-Ob_klu-E64 rv	pYS49	uYrdC_Ob_klu_K65A-W69A	amp121-128(TM62) antisense	pYS49				

### Supplementary Table 3: Primer list

Primer name	Sequence (5'-3')
amp121-128(TM62)	GCAGTGTGCCATAACCATGAGTG
amp121-128(TM62) antisense	CACTCATGGTTATGGCAGCACTGC
myc24 fw	GAACAAAACTCATCTCAGAAGAG
uYidC_Clo_klu_K65A-W69A	CCTAAAGACTATTTGGTCTATGAAGCATATAGAATAGCATGGTATTTTGTATATTTTAAA
uYidC-Clo_klu-E64 rv	TTCATAGACCAAATAGTCTTTAGGATA
Cd_AP_F76stp rv	ATCCTCTTCTGAGATGAGTTTTTGTCTTACAAACTACAATACCTCCAATATC
Cd_AP_F75stp rv	ATCCTCTTCTGAGATGAGTTTTTGTCTTAACTACAATACCTCCAATATCATA
Ck_AP_F76stp rv	ATCCTCTTCTGAGATGAGTTTTTGTCTTAAAAATATACAAAAATACCACCATAT
Ck_AP_F75stp rv	ATCCTCTTCTGAGATGAGTTTTTGTCTTAAATATACAAAAATACCACCATATTCT
Ck_AP_F74stp rv	ATCCTCTTCTGAGATGAGTTTTTGTCTTATACAAAAATACCACCATATTCTATA
lacZ lle4-fw	ATTACGGATTCACCTGGCCGT
PmifM-16nt 27rv	GCTTCATTTTACTATATGTACAAGCTG
C-kluyv-pCH746-fw	TACATATAGTAAATGAAGCTATTGAATGGATGTGATGAAAAAGACTCTATTAATAA
C-kluyv-pCH746 rv	ACGGCCAGTGAATCCGTAATCATGGTATTTAAAAATATGTTTCATATAAATCCTCTCCTTA
C_kluyv dele_TM12-21 fw	ATGAAAAAGACTCTATTAATAATGCAAAATCTGCTTTATGTTAGCACCATC
C_kluyv dele_TM12-21 rv	AATTTGCAATTATAATAGAGTATCTATTTTCAT
PT7-RBSkf-GFP	TAACTTTAAAGAAGGAGGGAGATATACCAATGACAATGTTTGTGGGATC
lacZ60-TAATAA-21-rv	TGGTGCCGGAACACAGGCAAATATTAGCGCCATTCGCCATTCAGGCT
Universal primer-77-PURE	GAAATTAATACGACTCACTATAGGGAGACCACAACGCGTTCCCTCTAGAAAAATTTTGTAACTTTAAGAAGGAG
amyE-front-fw	TAGAGATCCGATCAGACCAGT
flag-fw	GACTATAAAGACGACGACGAC
CliM-R71CGG-L75TTA-FLAG-fw	ATTTGGCGGTATTGTAGTTTATTTAAAGACTATAAAGAC
Cd_CliM-repro-KWm-fw	TTTCAGGCATATGATATTGCGCGGTATTGTAGTTTATTT
CliM-LacZ nonTGA fw	ATTTTAAAAAAGAACCATTGATTACGGATTCAGT
Cd_CliM-RE-77STP-FL-fw	GATATTTGGCGGTATTGTAGTTTATTTAAAGACTATAAAGACGAC
Cd_CliM-RE-L75A-77STP-FL-fw	GATATTTGGCGGTATTGTAGTGCATTTTAAAGACTATAAAGACGAC
Cd_CliM-RE-L75G-77STP-FL-fw	GATATTTGGCGGTATTGTAGTGGATTTTAAAGACTATAAAGACGAC
Ck_CliM-Dstem2-fw	GTATTTTGTATATTTTAAATTCGTTGAACAAGTAATATTTAGGAA
Cd_CliM-RE-76stp-FL-fw	GATATTTGGCGGTATTGTAGTTTATAATAAGACTATAAAGACGAC
Cd_CliM-S74L-76stp-FL-fw	GATATTTGGCGGTATTGTCTTTTATAATAAGACTATAAAGACGAC
Cd_CliM-S74G-76stp-FL-fw	GATATTTGGCGGTATTGTGGTTTATAATAAGACTATAAAGACGAC
Cd_CliM-S74V-76stp-FL-fw	GATATTTGGCGGTATTGTGTTTATAATAAGACTATAAAGACGAC
Cd_CliM-RE-L75DKK-77STP-FL-fw	GATATTTGGCGGTATTGTAGTDKKTTTTAAAGACTATAAAGACGAC
Cd_CliM-RE-L75S-77STP-FL-fw	GATATTTGGCGGTATTGTAGTTCATTTTAAAGACTATAAAGACGAC
Cd_CliM-RE-L75I-77STP-FL-fw	GATATTTGGCGGTATTGTAGTATATTTTAAAGACTATAAAGACGAC
Cd_CliM-RE-L75V-77STP-FL-fw	GATATTTGGCGGTATTGTAGTGTATTTTAAAGACTATAAAGACGAC
pDG1662-DspcR-fw	AATCAACGAGGTGAAATCGCTAATTTTATTGCAATAACA
gfp238-rv	TTTGTATAGTTCATCCATGCC
CliM-R71CGG-rv	ACTACAATACCGCCAAATATCATATTTCTGAAAAACTATATACTG
Cd_CliM-KWm-rv	CGCAATATCATATGCCGAAAAACTATATACTGTTAGG
Ck non TGA LacZ rv	CCGTAATCATGGTCTTATTTTAAAAATATACAAAAATACCA
Cd_CliM_RE-S74-rv	ACTACAATACCGCCAAATATCATATTT
Ck_CliM-Dstem2-rv	ATTTTAAAAATATACAAAAATACCA
Cd_CliM-C73-rv	ACAATACCGCCAAATATCATATTTCTG
pDG1662-DspcR-rv	TATTGCAATAAAATAGCGATTTTCACCTCGTTGATTATG
gfp238-fw	GGCATGGATGAACTATACAAA
FLAG_2-7-rv	TTTGTCTGCTCGTCTTTATA
Cdif_KYxIW-K-flag-rv	GTCGTCGCTTTATAGTCTTTTAAACAAACTACAATACCTCCAAT
FLAG-SpcR-fw	TATAAAGACGACGACGACAAAAGCAATTTAATTAACGGAAAA
amyE-SpcR-rv	ACTGGTCTGATCGGATCTCTACTAATTTAGAGAAAGTTTCTAT
Cd_AP_wt fw	GGCATGGATGAACTATACAAAAAGACCTCTTAAATCATAAAATTAAGTATGTT
Cd_AP_wt rv	ATCCTCTTCTGAGATGAGTTTTTGTCTTAAACAAACTACAATACCTCCAATATC
Cd_AP_stp77A rv	ATCCTCTTCTGAGATGAGTTTTTGTCTGCAACAAACTACAATACCTCCAAT
Cd_AP_stp77K rv	ATCCTCTTCTGAGATGAGTTTTTGTCTTAAACAAACTACAATACCTCCAATATC
Cdif AP Q65 rv	CTGAAAAACTATATACTGTTTAGGCAG
Cdif AP K66A W70A fw	CTGCCTAAACAGTATATAGTTTTTCAGGCATATGATATTGCGAGGTATTGTAGTTTGTAAAGAA

## Supplementary Table 4: Degenerate primers for DMS

Primer name	Sequence (5'-3')
Cdif_KYx1w_K77-NNK-fw2nd	TGGCGGTATTGTAGTTTATTNNKGACTIONATAAAGACGAC
Cdif_KYx1w_F76-NNK-fw2nd	ATTTGGCGGTATTGTAGTTTANNKAAAGACTATAAAGAC
Cdif_KYx1w_L75-NNK-fw2nd	GATATTTGGCGGTATTGTAGTNNKTTAAAGACTATAAA
Cdif_KYx1w_S74-NNK-fw2nd	TATGATATTTGGCGGTATTGTNNKTTATTTAAAGACTAT
Cdif_KYx1w_C73-NNK-fw2nd	AAATATGATATTTGGCGGTATNNKAGTTTATTAAAGAC
Cdif_KYx1w_Y72-NNK-fw2nd	CAGAAATATGATATTTGGCGGNKGTAGTTTATTTAAA
Cdif_KYx1w_R71-NNK-fw2nd	TTTCAGAAATATGATATTTGGNNKATTTAGTATTTATTT
Cdif_KYx1w_W70-NNK-fw2nd	GTTTTTCAGAAATATGATATTTNNKCGGTATTGTAGTTTA
Cdif_KYx1w_I69-NNK-fw2nd	ATAGTTTTTCAGAAATATGATNNKTTGGCGGTATTGTAGT
Cdif_KYx1w_D68-NNK-fw2nd	TATATAGTTTTTCAGAAATATNNKATTTGGCGGTATTGT
Cdif_KYx1w_Y67-NNK-fw2nd	CAGTATATAGTTTTTCAGAAANNKATATTTGGCGGTAT
Cdif_KYx1w_K66-NNK-fw2nd	AAACAGTATAGTTTTTCAGNNKATGATATTTGGCGG
Cdif_KYx1w_Q65-NNK-fw	CCTAAACAGTATAGTTTTNNKAAATATGATATTTGG
Cdif_KYx1w_F64-NNK-fw	CTGCCTAAACAGTATAGTTNNKAGAAATATGATAT
Cdif_KYx1w_V63-NNK-fw	CGACTGCCTAAACAGTATATANNKTTTCAGAAATATGAT
Cdif_KYx1w_I62-NNK-fw	GAACGACTGCCTAAACAGTATNNKGTTTTTTCAGAAATAT
Cdif_KYx1w_Y61-NNK-fw	GAAGAAGACTGCCTAAACAGNNKATAGTTTTTCAGAAA
Cdif_KYx1w_Q60-NNK-fw	TCTGAAGAAGACTGCCTAAANNKATATAGTTTTTCAG
Cdif_KYx1w_K59-NNK-fw	TATTTCTGAAGAAGACTGCCTNNKAGTATATAGTTTTT
Cdif_KYx1w_P58-NNK-fw	ACATATTTCTGAAGAAGACTGNNKAAACAGTATATAGTT
Cdif_KYx1w_L57-NNK-fw	ATTACATATTTCTGAAGAAGANNKCTAAACAGTATATA
Cdif_KYx1w_R56-NNK-fw	AGAATTACATATTTCTGAAGAANNKCTGCCTAAACAGTAT
Cdif_KYx1w_E55-NNK-fw	AATAGAATTACATATTTCTGAANNKCGACTGCCTAAACAG
Cdif_KYx1w_E54-NNK-fw	GTAAATAGAATTACATATTTCTNNKGAACGACTGCCTAAA
Cdif_KYx1w_S53-NNK-fw	TTTTGTAATAGAATTACATATNNKGAAGAAGACTGCCT
Cdif_KYx1w_Y52-NNK-fw	ATATTTGTAAATAGAATTACANNKCTGAAGAAGACTGC
Cdif_KYx1w_T51-NNK-fw	GACATATTTGTAAATAGAATTNNKATTTCTGAAGAAGCA
Cdif_KYx1w_I50-NNK-fw	AGAGACATATTTGTAAATAGANNKACATATTTCTGAAGAA
Cdif_KYx1w_R49-NNK-fw	ATAAGAGACATATTTGTAAATNNKATTTACATATTTCTGAA
Cdif_KYx1w_N48-NNK-fw	TTAATAAGAGACATATTTGTANNKAGAATTACATATTTCT
Cdif_KYx1w_V47-NNK-fw	GTTTTAATAAGAGACATATTTNNKAAATAGAATTACATAT
Cdif_KYx1w_F46-NNK-fw	TATGTTTTAATAAGAGACATANNKGTAAATAGAATTACA
Cdif_KYx1w_I45-NNK-fw	AAGTATGTTTTAATAAGAGACNNKTTTGTAAATAGAATT
Cdif_KYx1w_D44-NNK-fw	ATTAAGTATGTTTTAATAAGANNKATATTTGTAAATAGA
Cdif_KYx1w_R43-NNK-fw	AAAATTAAGTATGTTTTAATANNKAGACATATTTGTAAAT
Cdif_KYx1w_V42-NNK-fw	CATAAAATTAAGTATGTTTTANNKAGAGACATATTTGTA
Cdif_KYx1w_L41-NNK-fw	AATCATAAAATTAAGTATGTTNNKATAAGAGACATATTT
Cdif_KYx1w_V40-NNK-fw	TTAAATCATAAAATTAAGTATNNKTTAATAAGAGACATA
Cdif_KYx1w_Y39-NNK-fw	CTCTTAAATCATAAAATTAAGNNKGTTTTTAATAAGAGAC
Cdif_KYx1w_K38-NNK-fw	GACCTCTTAAATCATAAAATNNKATGTTTTAATAAGAA
Cdif_KYx1w_L75-rv2nd	TAAACTACAATACCGCCAAATATCATA
Cdif_KYx1w_C73-rv2nd	ACAATACCGCCAAATATCATAATTTCTG
Cdif_KYx1w_R71-rv2nd	CCGCCAAATATCATAATTTCTGAAAAAC
Cdif_KYx1w_I69-rv	AATATCATAATTTCTGAAAAACTATATA
Cdif_KYx1w_Y67-rv	TTTCTGAAAAACTATATACTGTTTAGG
Cdif_KYx1w_Q65-rv	CTGAAAAACTATATACTGTTTAGGCAG
Cdif_KYx1w_V63-rv	TATATACTGTTTAGGCAGTCGTTCTTC
Cdif_KYx1w_Y61-rv	CTGTTTAGGCAGTCGTTCTTCAGAATA
Cdif_KYx1w_K59-rv	AGGCAGTCGTTCTTCAGAATATGTAAT
Cdif_KYx1w_L57-rv	TCGTTCTTCAGAATATGTAATTTCTATT
Cdif_KYx1w_E55-rv	TTCAGAATATGTAATTTCTATTACAAA
Cdif_KYx1w_S53-rv	ATATGTAATTTCTATTACAAATATGTC
Cdif_KYx1w_T51-rv	AATTTCTATTACAAATATGTTCTTTAT
Cdif_KYx1w_R49-rv	ATTTACAAATATGTTCTTTATTAAC
Cdif_KYx1w_V47-rv	AAATATGTTCTTTATTAACATACTT
Cdif_KYx1w_I45-rv	GTCTCTTATTAACATACTTAAATTT
Cdif_KYx1w_R43-rv	TCTTATTAACATACTTAAATTTATG
Cdif_KYx1w_L41-rv	AACATACTTAAATTTATGATTTAAGAG
Cdif_KYx1w_Y39-rv	CTTAATTTATGATTTAAGAGGTCCTT
Cdif_KYx1w_I37-rv	AATTTATGATTTAAGAGGTCCTTTTT

**Supplementary Table 5: Primers used for preparation of NGS library**

Primer name	Sequence(5'-3')
P5-UDI0001-Rd1-TAG-gfp215-fw	AATGATACGGCGACCACCGAGATCTACACAGCGCTAGACACTCTTCCCTACACGACGCTC TTCCGATCTNNNNNNTAGAGAGACCACATGGTCCTTCTT
P7-UDI0001-Rd2-ACC-FLAG2-8-rv	CAAGCAGAAGACGGCATAACGAGATAACCGCGGGTGACTGGAGTTCAGACGTGTGCTCTTC CGATCTNNNNNNACCTTTGTCGTCGTCGTCCTTTATA
P7-UDI0001-Rd2-AGC-FLAG2-8-rv	CAAGCAGAAGACGGCATAACGAGATAACCGCGGGTGACTGGAGTTCAGACGTGTGCTCTTC CGATCTNNNNNNAGCTTTGTCGTCGTCGTCCTTTATA
P7-UDI0001-Rd2-AGG-FLAG2-8-rv	CAAGCAGAAGACGGCATAACGAGATAACCGCGGGTGACTGGAGTTCAGACGTGTGCTCTTC CGATCTNNNNNNAGGTTTGTGTCGTCGTCGTCCTTTATA
P7-UDI0001-Rd2-CTC-FLAG2-8-rv	CAAGCAGAAGACGGCATAACGAGATAACCGCGGGTGACTGGAGTTCAGACGTGTGCTCTTC CGATCTNNNNNNCTCTTTGTGTCGTCGTCGTCCTTTATA
P7-UDI0001-Rd2-CTG-FLAG2-8-rv	CAAGCAGAAGACGGCATAACGAGATAACCGCGGGTGACTGGAGTTCAGACGTGTGCTCTTC CGATCTNNNNNNCTGTTTGTGTCGTCGTCGTCCTTTATA
P7-UDI0001-Rd2-TGC-FLAG2-8-rv	CAAGCAGAAGACGGCATAACGAGATAACCGCGGGTGACTGGAGTTCAGACGTGTGCTCTTC CGATCTNNNNNNTGCTTTGTGTCGTCGTCGTCCTTTATA
P7-UDI0001-Rd2-TTA-FLAG2-8-rv	CAAGCAGAAGACGGCATAACGAGATAACCGCGGGTGACTGGAGTTCAGACGTGTGCTCTTC CGATCTNNNNNNTTATTTGTGTCGTCGTCGTCCTTTATA
P7-UDI0001-Rd2-TTG-FLAG2-8-rv	CAAGCAGAAGACGGCATAACGAGATAACCGCGGGTGACTGGAGTTCAGACGTGTGCTCTTC CGATCTNNNNNNTTGTTTGTGTCGTCGTCGTCCTTTATA

**Supplementary Table 6: MD simulation checklist.**

<b>Reliability and reproducibility checklist for molecular dynamics simulations</b> <b>*All boxes must be marked YES by acceptance unless an N/A option is available</b>	<b>Yes</b>	<b>N/A</b>	<b>Response</b> <b>(Please state where this information can be found in the text)</b>
<b>1. Convergence of simulations and analysis</b>			
1a. Is an evaluation presented in the text to show that the property being measured has equilibrated in the simulations ( <i>e.g.</i> time-course analysis)?	<input checked="" type="checkbox"/>		See ED Fig. 7b
1b. Then, is it described in the text how simulations are split into equilibration and production runs and how much data were analyzed from production runs?	<input checked="" type="checkbox"/>		See Methods: MD simulation Set-up
1c. Are there at least 3 simulations per simulation condition with statistical analysis?	<input checked="" type="checkbox"/>		10 replica simulations per condition each. See Methods: MD simulation setup.
1d. Is evidence provided in the text that the simulation results presented are independent of initial configuration?	<input checked="" type="checkbox"/>		Evidence is provided in Figure 8a, showing that a wide conformational space around the cryo-EM model is explored by CliM NC.
<b>2. Connection to experiments</b>			
2a. Are calculations provided that can connect to experiments ( <i>e.g.</i> loss or gain in function from mutagenesis, binding assays, NMR chemical shifts, J-couplings, SAXS curves, interaction distances or FRET distances, structure factors, diffusion coefficients, bulk modulus and other mechanical properties, <i>etc.</i> )?	<input checked="" type="checkbox"/>		Mutagenesis experiments of stalling critical residue L75 (Fig. 7) were complemented and compared with MD simulations (Fig. 8a).
<b>3. Method choice</b>			
3a. Is it described in the text what force field and water model are used and why?	<input checked="" type="checkbox"/>		See Methods: MD simulation Set-up
3b. Do simulations contain membranes, membrane proteins, intrinsically disordered proteins, glycans, nucleic acids, polymers, or cryptic ligand binding?	<input checked="" type="checkbox"/>	<input type="checkbox"/>	Nucleic acids

	If 3b is <b>YES</b> , are enhanced sampling methods used?	<input type="checkbox"/>	<input checked="" type="checkbox"/>	Response not needed if <b>N/A</b>
	If enhanced sampling methods are used, are the convergence criteria clearly stated?	<input type="checkbox"/>		
	If 3b is <b>YES</b> , is it explained in the text why or why not enhanced sampling methods are used?	<input type="checkbox"/>		
<b>4. Code and reproducibility</b>				
	4a. Is a table provided describing the system setup, such as simulation box dimensions, total number of atoms, total number of water molecules, salt concentration, lipid composition (number of molecules and type)?	<input checked="" type="checkbox"/>		See Methods: MD simulation setup.
	4b. Is it described in the text what simulation and analysis software and which versions are used?	<input checked="" type="checkbox"/>		See Methods: MD simulation setup.
	4c. Are initial coordinate and simulation input files and a coordinate file of the final output provided as supplementary files or in a public repository?	<input checked="" type="checkbox"/>		<a href="https://doi.org/10.5281/zenodo.17779011">https://doi.org/10.5281/zenodo.17779011</a>
	4d. Is there custom code or custom force field parameters?	<input type="checkbox"/>	<input checked="" type="checkbox"/>	Response not needed if <b>N/A</b>
	If <b>YES</b> , are they provided as supplementary profiles or in a public repository?	<input type="checkbox"/>		

## Supplementary References

1. Syroegin, E. A., Aleksandrova, E. V & Polikanov, Y. S. Insights into the ribosome function from the structures of non-arrested ribosome-nascent chain complexes. *Nat. Chem.* 15, 143–153 (2023).
2. Gersteuer, F. *et al.* The SecM arrest peptide traps a pre-peptide bond formation state of the ribosome. *Nat. Commun.* 15, 2431 (2024).
3. Su, T. *et al.* The force-sensing peptide VemP employs extreme compaction and secondary structure formation to induce ribosomal stalling. *Elife* 6, (2017).
4. van der Stel, A.-X. *et al.* Structural basis for the tryptophan sensitivity of TnaC-mediated ribosome stalling. *Nat. Commun.* 12, 5340 (2021).
5. Matheisl, S., Berninghausen, O., Becker, T. & Beckmann, R. Structure of a human translation termination complex. *Nucleic Acids Res.* 43, 8615–26 (2015).
6. Aleksandrova, E. V *et al.* Mechanism of release factor-mediated peptidyl-tRNA hydrolysis on the ribosome. *Science* 388, eads9030 (2025).
7. Beckert, B. *et al.* Structural and mechanistic basis for translation inhibition by macrolide and ketolide antibiotics. *Nat. Commun.* 12, 4466 (2021).